Deep-Sea Research I 114 (2016) 111–127

Contents lists available at ScienceDirect

Deep-Sea Research I

journal homepage: www.elsevier.com/locate/dsri

Bio-optical characterization of offshore NW Mediterranean waters: CDOM contribution to the absorption budget and diffuse attenuation of downwelling irradiance

Gonzalo L. Pérez [a,*], Martí Galí [b,c], Sarah-Jeanne Royer [b], Hugo Sarmento [d], Josep M. Gasol [b], Cèlia Marrasé [b], Rafel Simó [b]

[a] Instituto INIBIOMA (CRUB Comahue, CONICET), Quintral 1250, 8400 S.C. de Bariloche, Rio Negro, Argentina
[b] Institut de Ciències del Mar, CSIC, Passeig Marítim de la Barceloneta 37-49, 08003 Barcelona, Catalonia, Spain
[c] Takuvik Joint International Laboratory and Québec-Océan, Université Laval, Québec, QC, Canada G1V OA6
[d] Laboratory of Microbial Processes and Biodiversity, Department of Hydrobiology, Federal University of São Carlos, São Carlos, Brazil

ARTICLE INFO

Article history:
Received 2 September 2015
Received in revised form
5 May 2016
Accepted 29 May 2016
Available online 7 June 2016

ABSTRACT

We investigated the peculiar bio-optical characteristics of the Mediterranean Sea focusing on the spectral diffuse attenuation coefficient [Kd (λ)] and its relationship with chlorophyll *a* concentration (Chl *a*), complemented with measurements of light absorption by chromophoric dissolved organic matter (CDOM) and the optical properties of particulate material. The non-water absorption budget showed that CDOM was the largest contributor in the 300–600 nm range (> 60% of the absorption at 443 nm in the euphotic layer), increasing to 80% within the first optical depth (FOD). This translated into CDOM accounting for > 50% of Kd_{Bio} (λ) (the irradiance attenuation coefficient caused by all non-water absorptions) between 320 and 555 nm and throughout both layers (FOD and euphotic). Indeed, we tested three Chl *a*-based bio-optical models and all three underestimated Kd (λ), evidencing the importance of CDOM beside Chl *a* to fully account for light attenuation. The Morel & Maritorena (2001) model (M&M 01) underestimated Kd (λ) in the UV and blue spectral regions within the FOD layer, showing lower differences with increasing wavelengths. The Morel et al. (2007a) model (BGS 07) also underestimated Kd (λ) in the FOD layer, yet it performed much better in the 380–555 nm range. In the euphotic layer, the Morel (1988) model (JGR 88) underestimated Kd (λ) showing higher differences at 412 and 443 nm and also performed better at higher wavelengths. Observed euphotic layer depths ($Z_{1\%}$) were 28 m shallower than those predicted with the M&M 01 empirical relationship, further highlighting the role of CDOM in the bio-optical peculiarity of Mediterranean Sea. *In situ* measurements of the CDOM index (Φ), an indicator of the deviation of the CDOM-Chl *a* average relationship for Case 1 waters, gave a mean of 5.9 in the FOD, consistent with simultaneous estimates from MODIS (4.8 ± 0.4). The implications of the bio-optical anomaly for ecological and biogeochemical inferences in the Mediterranean Sea are discussed.

1. Introduction

In ocean bio-optics, Case 1 waters are those whose optical properties are determined primarily by phytoplankton and the associated detrital particles and dissolved materials, to the extent that they can be described and modelled solely from phytoplankton chlorophyll *a* concentration (Chl *a*) (Morel and Prieur, 1977; Antoine et al., 2014). In these waters, inherent optical properties (IOPs) such as phytoplankton absorption coefficients (e.g., Bricaud et al., 1995, 1998, 2004; Stæhr and Markager, 2004) or particle scattering and beam attenuation coefficients (e.g., Gordon and Morel, 1983; Voss, 1992; Loisel and Morel, 1998; Loisel et al., 2011) have been statistically related to Chl *a*. And so have been apparent optical properties (AOPs) such as the diffuse attenuation coefficient (Kd) and reflectance (R) (e.g., Morel, 1988; Morel and Maritorena, 2001; Morel and Gentili, 2004; Morel et al., 2007a). However, several studies in Case 1 waters have shown significant deviations of the optical data from the most used empirical and semiempirical relationships to Chl *a* concentration (e.g., Mitchell and Holm-Hansen, 1991; Morel et al., 2007a,b ; Loisel et al., 2011; Antoine et al., 2013; Organelli et al., 2014). Such deviations occur systematically in some regions like, e.g., the South Pacific and the Mediterranean Sea (Morel et al., 2007a; Morel and Gentili, 2009a,b).

* Corresponding author.
E-mail address: perezgonzaloluis@gmail.com (G.L. Pérez).

http://dx.doi.org/10.1016/j.dsr.2016.05.011
0967-0637/

In the Mediterranean, application of global algorithms to satellite ocean color data results in notable and recurrent overestimation of the in situ Chl *a* concentration (Antoine et al., 1995; Gitelson et al., 1996; Bricaud et al., 2002; Volpe et al., 2007; Antoine et al., 2008). Overestimation also occurs when the same algorithms are fed with in situ spectral measurements of water leaving radiances, indicating that optical constituents other than Chl *a* decrease the blue-to-green reflectance ratio (B/G) (Claustre et al., 2002; Quillon and Petrenko, 2005). Among the possible causes of this color anomaly, high concentrations of CDOM have been frequently invoked (e.g., Morel et al., 2007a; Morel and Gentili, 2009b). Other possible causes are the deposition of submicron-sized Saharan dust, which would result in an enhancement of the backscattering coefficient at the green portion of the spectrum (Claustre et al., 2002; Loisel et al., 2011), and the higher relative abundance of coccolithophorid microalgae amongst Mediterranean phytoplankton (Gitelson et al., 1996; D'Ortenzio et al., 2002).

CDOM consists of optically active material that strongly absorbs in the blue (e.g., 443 nm). It does not always correlate with other biogenic components; instead, its own dynamics and its varying contribution to the light absorption budget confounds the classical B/G algorithms used to retrieve Chl *a* concentration from remote sensing platforms (Claustre and Maritorena, 2003; Siegel et al., 2005; Morel and Gentili, 2009b). Ocean color data reveal that Mediterranean waters contain on average twice the CDOM expected from their Chl *a* content (Morel and Gentili, 2009a,b). A study that focused on the parameterization of Kd (λ) using Chl *a* concentration, also sustained this suggestion (Morel et al., 2007a). *In situ* measurements have shown indeed that Kd values between 320 and 440 nm are recurrently high in relation to those predicted from the Chl *a* concentration using Case 1 waters algorithms. This anomaly was found to steadily increase with decreasing wavelengths (maximum differences at 320 nm), which is a typical signature of the CDOM absorption spectrum [a_{cdom} (λ)] (Morel et al., 2007a). These authors also pointed out that the depths of 1% irradiance ($Z_{1\%}$) are considerably shallower than those predicted from depth-integrated Chl *a*, and concluded that specific parameterizations for Kd (λ) are needed for Mediterranean waters (Morel et al., 2007a).

Despite these findings, only a limited number of field determinations of CDOM absorption characteristics have been conducted in costal (e.g., Babin et al., 2003; Vignudelli et al., 2004; Para et al., 2010; Romera-Castillo et al., 2011; Romera-Castillo et al., 2013) and offshore Mediterranean waters (Kitidis et al., 2006; Bracchini et al., 2010; Xing et al., 2014; Organelli et al., 2014). Only a few assessed the spatial and seasonal dynamics of in situ CDOM absorption coefficients together with their drivers. Xing et al. (2012, 2014) reported a substantial asymmetry of CDOM levels between the Western and the Eastern basins, with higher values in the former, and also observed different seasonal dynamics between surface and subsurface CDOM standing stocks and their physical and biological drivers (Xing et al., 2014). In the NW Mediterranean, Organelli et al. (2014) confirmed that the values of a_{cdom} (440) for a given Chl *a* concentration were higher than those expected for Case 1 waters, and showed that CDOM dominated the non-water light absorption budget of surface waters throughout most of the year.

Here we examine in detail the role of CDOM in the not fully understood bio-optical peculiarity of the Mediterranean Sea. We focus particularly on the Kd (λ) to Chl *a* relationship, complemented with a comprehensive optical characterization of CDOM and particulate material (phytoplankton and non-algal particles). Using data obtained during two Lagrangian cruises in offshore waters of the NW Mediterranean, we aimed to: (i) describe the spectral absorption coefficients of the various optically active components in the near-UV and visible spectral domains; (ii) assess their relative contribution to the light absorption budget; (iii) evaluate the contributions of absorption and scattering to irradiance attenuation in the FOD and euphotic layers by modelling and partitioning of Kd (λ) using Kirk's optical model (Kirk, 1991); (iv) evaluate the performance of Chl *a*-based models of light attenuation, namely the widely used JGR 88 (Morel, 1988) and M&M 01 (Morel and Maritorena, 2001), as well as the regionally tuned BGS 07 model (Morel et al., 2007a); and (v) assess the implications of the bio-optical peculiarity for an accurate description of optical properties of the Mediterranean Sea, and provide information for the improvement of bio-optical models and remote sensing applications in marine ecology and biogeochemistry.

2. Materials and methods

2.1. Study area and sampling

Data were collected in offshore waters of the Catalan-Balearic Sea (NW Mediterranean) during two Lagrangian cruises, denoted SUMMER-1 (SU1) and SUMMER-2 (SU2), on 12-22 Sept 2011 and 22-24 May 2012, respectively.

The two cruises were conducted on board the RV 'García del Cid'. Three Lagrangian drifters were deployed to track the movement of the upper 15-m water layer. Each drifter consisted of a spherical floatable enclosure that contained a GPS and an emitter, from which 10 m cylindrical drogues hanged 5 m below the sphere. The drifters sent their position every 30 min, and all ship operations were conducted next to them. Both cruises were held in the same region, ca. 45 nautical miles from the coast, within the core of a cyclonic eddy over a water-column depth of ca. 2000 m (Fig. 1). Measurements were obtained from a total of 28 stations (21 and 6 on SU1 and SU2, respectively). Vertical profiles were acquired with a Seabird 9/11 plus CTD probe equipped with a PAR radiometer (QCP-2300, Biospherical), chlorophyll fluorometer (Seapoint) and transmissometer (C-Star WETLabs). The CTD system was mounted on a 24-Niskin-bottle rosette used to collect, at each station, water samples at fixed depths plus an additional sample at the depth where the deep chlorophyll maximum (DCM) was detected on the basis of real-time fluorescence profiles. In SU1 four depths were sampled (3, 8 or 10, 30 m and DCM), and 3 in SU2 (3, 25 m and DCM). Mixed layer depths (MLD) were estimated from CTD temperature profiles, and defined by a ≥ 0.2 °C deviation with respect to the temperature at 1 m depth.

Vertical profiles of downwelling spectral irradiance E_d (λ, Z) at 6 discrete channels in the ultraviolet region (305, 313, 320, 340, 380 and 395 nm) and 9 channels in the visible wavelengths matching the band position of remote sensing platforms (412, 443, 465, 490, 510, 555, 670, 694 and 710 nm), as well as the integrated PAR band [E_d (PAR, Z)], were measured with a PRR-800 multichannel profiling radiometer (Biospherical). The radiometer was deployed once a day during both cruises, with the exception of two days of SU1 when weather conditions prevented optical profiles. Prior to each cast, the ship was oriented relative to the sun to minimize ship shadow. A total of 12 irradiance profiles were carried out with solar angles ranging from 24° to 54° and recorded from the surface to 100 m. All the irradiance profiles (with PRR-800 radiometer and CTD casts) were carried out on calm days, during clear sky and constant light conditions. Incident surface PAR irradiance in air was simultaneously monitored with an on-deck global solar radiation sensor (# 6450, Davis sensor), and used to verify that the above-water surface irradiance was constant during profiling.

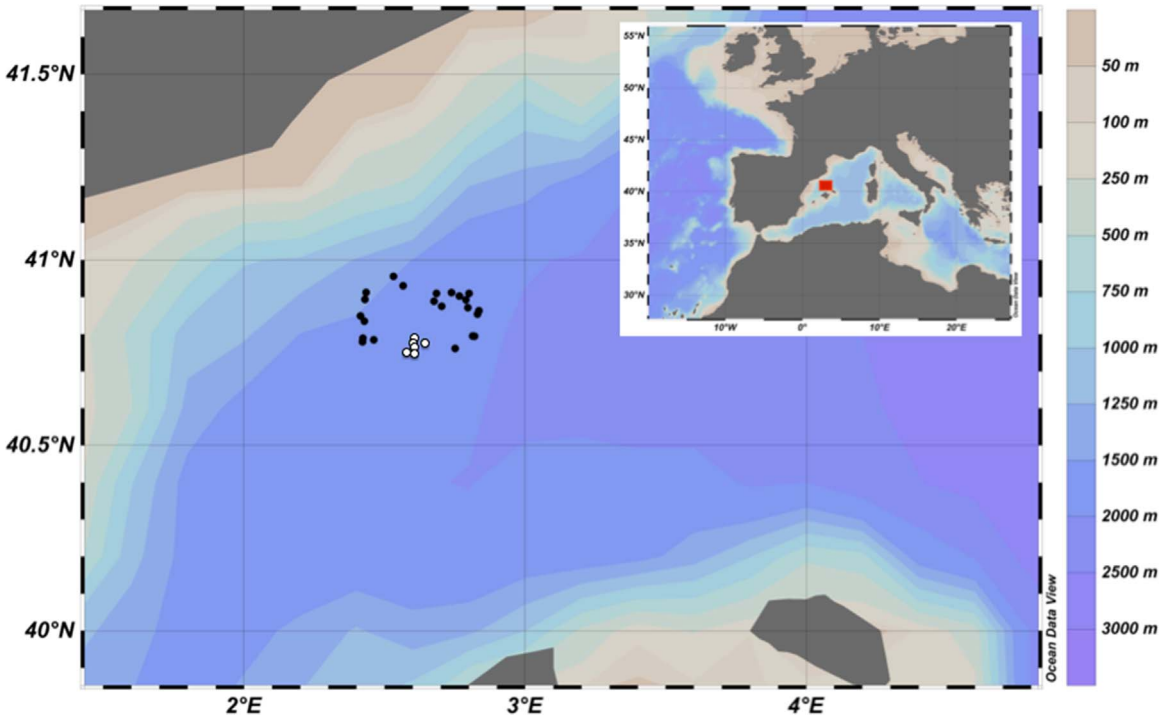

Fig. 1. Map showing the stations sampled in the two SUMMER cruises: SU1 (black dots) and SU2 (white dots).

2.2. Apparent optical properties measurements: diffuse attenuation coefficients for downwelling irradiance

Average diffuse attenuation coefficients in the euphotic zone, for discrete wavelengths (derived from PRR-800 Ed profiles) and for the PAR broadband (from both CTD and PRR-800 Ed profiles), were determined as the slope of the linear regression between logarithmic irradiances and depth. Quality- control of radiometric data was performed according to Mueller et al. (2003). Near-surface noise caused by wave motion was eliminated from E_d (λ, PAR, Z) profiles. At each UV wavelength (from 320 to 395 nm), the maximum depth considered for calculation was determined by the break of the Ln [E_d (λ)] vs. depth curve (i.e., when the Kd changed through the water column), being the subsequent portion of the curve excluded from calculations (see Laurion et al. (2000)). For wavelengths between 412 and 555 nm and for the PAR band, the maximum depth considered for calculations was the depth where approximately 1% of subsurface E_d (λ, PAR) remained. For wavelengths > 600 nm, we followed the same approach as for UV, considering for slope calculation the curve before the change of Kd through the water column. A similar procedure was employed by Morel (1988), with Kd in the red part of the spectrum computed by considering a layer with a reduced thickness. We also followed the same procedure (linear regression analysis) in the calculation of Kd for the FOD layer, whose depth was estimated as 1/Kd (PAR). The R^2 obtained from regression analyses were always above 0.98 at all examined wavelengths and casts. The depth of the euphotic layer was calculated as 4.605/Kd (PAR), which is the depth at which PAR is 1% of the value just below the surface.

2.3. Laboratory measurements

2.3.1. Inherent optical properties

Absorption by CDOM in discrete water samples (n = 106) was characterized by UV–visible spectrophotometric scans performed on seawater filtered through pre-combusted (450 °C, 4 h.) Whatman GF/F filters, in an acid-cleaned all-glass filtration system and under positive pressure with low N_2 flow. Although dissolved matter is generally defined as that passing through a 0.2-μm membrane (Mueller and Austin, 1995), and the nominal pore size of GF/F filters is ca. 0.7 μm, this is known to decrease in the pre-combustion process, thus making GF/F appropriate for measurement of dissolved organics avoiding organic membranes (Nayar and Chou, 2003; Asmala et al., 2012). CDOM absorbance was measured in a Lambda 800 (Perkin-Elmer) dual beam spectrophotometer equipped with a 10 cm quartz cell. Spectral scans between 250 and 750 nm at 1 nm intervals were made on-board immediately after filtration. Pre-filtered (0.2 μm) Milli-Q water was used as the reference for all samples. The CDOM absorption coefficients were calculated as follows:

$$a_{cdom}(\lambda) = 2.303.\frac{A_{filtrate}(\lambda)}{l} \quad (1)$$

where $A_{filtrate}$ (λ) is the absorbance at wavelength λ, and l is the cell length in metres. The spectra were corrected for residual scattering by fine size particles, micro-air bubbles, or refractive index differences between the sample and the reference by subtracting the average value of absorbance between 600 and 720 nm (Mitchell et al., 2000). Given the detection limit of the spectrophotometer (0.001 absorbance units) and an optical cell pathlength of 0.1 m, the detection limit for CDOM absorption was 0.02 m^{-1}.

Following Helms et al. (2008), CDOM spectral slopes were calculated over four narrow wavelength ranges: $S_{275–295}$, $S_{290–350}$, $S_{350–400}$ and $S_{350–500}$, using linear regressions of the natural log-transformed a_{cdom} (λ) spectra. In addition, we also calculated the dimensionless $S_{275–295}/S_{350–400}$ (denoted S_R), and a_{cdom} (250/365) ratios.

In the same discrete water samples, total particulate matter absorption coefficients [a_p (λ)] were determined by the quantitative filter technique (QFT) using the simple transmittance method according to NASA's optics protocols (Mitchell et al., 2000). Water samples (1–2 L) were filtered on-board using 25 mm GF/F filters. Immediately after filtration absorbance scans were measured from

300 to 750 nm at 1 nm intervals in a Lambda 800 spectrophotometer against a blank clean filter wetted with filtered (0.2 μm) seawater. Absorption coefficients of non-algal particles [a_{nap} (λ)] (i.e., non-chlorophyllic, unpigmented particles) were determined after methanol extraction following the procedure of Kishino et al. (1985). Absorption coefficients of a_p (λ) (first measurement) and a_{nap} (λ) (after methanol extraction) were estimated according the equation:

$$a_{p,nap}(\lambda) = \frac{2.303.A_{filter}(\lambda).S}{V.\beta(\lambda)} \quad (2)$$

where A_{filter} (λ) is the measured absorbance with QFT, S is the clearance area of the filter, V is the volume of filtered water, and β (λ) is the amplification factor vector (Mitchell and Kiefer, 1984). The β (λ) factor was calculated following Bricaud and Stramski (1990) with the equation:

$$\beta(\lambda)=1.63.A_{filter}(\lambda)^{-0.22} \quad (3)$$

As standard procedure, a null point correction was set at 750 nm, where absorbance by particles is assumed to be negligible. This was done to correct for residual offsets in the sample filter relative to the reference, and for scattering artifacts due to particle loading (Mitchell et al., 2000). Phytoplankton absorption coefficients [a_{ph} (λ)] were obtained by subtracting a_{nap} (λ) from a_p (λ). Finally, total absorption coefficients [a_t (λ)] were estimated as the sum of the absorption coefficients by particles, CDOM and pure water:

$$a_t(\lambda) = a_{cdom}(\lambda) + a_p(\lambda) + a_w(\lambda) \quad (4)$$

where a_w (λ), the absorption coefficient of pure water, was taken from Pope and Fry (1997) and from Morel et al. (2007b) for the UV-blue range (see a_{w1} values in Morel et al. (2007b)).

The particulate spectral scattering coefficient [b_p (λ)] was obtained from the difference between beam attenuation coefficient by particles [c_p (660)] and spectral particulate absorption coefficients following Roesler and Boss (2003):

$$b_p(\lambda) = c_p(660)\cdot\left[\frac{\lambda}{660}\right]^{-1} - a_p(\lambda) \quad (5)$$

Particulate beam attenuation at each sampling depth was calculated from 1 m binned transmittance vertical profiles and determined subtracting the mean value of beam attenuation over the depth interval from 200 to 400 m, which was considered representative of the beam attenuation value of particle-free water (depth-independent background) (Loisel and Morel, 1998; Loisel et al., 2011). The spectral dependence of the beam attenuation coefficient was obtained using a λ^{-1} dependency. Oubelkheir et al. (2005) reported a spectral particle attenuation exponent ranging from about 1–1.5 for NW Mediterranean waters.

The total spectral scattering coefficient [b (λ)] was obtained as: b_p (λ)+b_w (λ), where b_w (λ) is the scattering coefficient of pure water derived from Buiteveld (1994) and multiplied by 1.30 to account for the effect of salinity (see Morel et al. (2007a)).

2.3.2. Pigment analysis

Samples for pigment analyses were collected from Niskin bottles (1.5–2 L), filtered through Whatman GF/F filters and stored at −80 °C until analysis in the laboratory on land. Total Chl*a* concentration (hereinafter denoted T-Chl *a*, which includes Chl *a*+allomers and epimers+divinyl Chl *a*+chlorophyllide *a*) was measured by High Performance Liquid Chromatography (HPLC) on a Spectra SYSTEM instrument following the method of Zapata et al. (2000). Calibration was done with commercial pigment standards (DHI, Denmark). Vertical profiles of chlorophyll fluorescence recorded during CTDs casts were calibrated and subsequently converted into equivalent T-Chl *a* profiles by using the HPLC concentration values obtained in discrete samples.

2.4. Description of diffuse attenuation coefficient modelling

2.4.1. Kirk's optical model of Kd (λ)

The diffuse attenuation coefficient for the euphotic layer was modelled using Kirk´s optical model (Kirk, 1981; 1984; 1991), which has been successfully used to model Kd (λ) in a wide range of aquatic environments (Bricaud et al., 1998; Gallegos, 2001; Belzile et al., 2002; MacIntyre et al., 2004; Pierson et al., 2008; Zhang et al., 2009) and is particularly useful because of its simplicity and accuracy. The model relates the average attenuation coefficient of downwelling irradiance in the euphotic zone as an explicit function of a, b, and μ_0 as follows:

$$Kd(\lambda) = \frac{1}{\mu_0}\cdot\left\{a_t(\lambda)^2 + G(\mu_0)\cdot a_t(\lambda)\cdot b(\lambda)\right\}^{0.5} \quad (6)$$

where μ_0 is the average cosine of the angle of the stream of photons just under the surface (calculated from the incident zenith angle using Snell's Law), and G (μ_0) is a coefficient that indicates the relative contribution of scattering to vertical irradiance attenuation determined by the shape of the volume scattering function [β (θ)] and by μ_0. G (μ_0) is a linear function of μ_0 as: G (μ_0)=g_1.μ_0-g_2. The coefficients g_1 and g_2 vary with the shape of the volume scattering function used in the calculations (Kirk, 1991). We used g_1=0.425 and g_2=0.19, for San Diego Harbour scattering phase function obtained from Monte Carlo calculations (Kirk, 1991, 2011). We also used Kirk´s model for modelling Kd (λ) in the FOD layer. In this case we followed a simplified approach, using G (1)=0.126 (see Kirk (1991)).

Mean observed values of a_t (λ) and b (λ), either in the euphotic layer or in the FOD layer, were used as input values for the model. Then the model was run to determine the relative contribution of absorption and scattering to light attenuation. Following procedures set forth by Belzile et al. (2002; see their Models I, II and III), the relative contribution of IOPs (absorption and scattering by different components) to Kd were computed.

2.4.2. Chl a-based models of Kd (λ)

The JGR88 model statistically relates Kd_{Bio} (=Kd (λ)-Kd_w (λ)) in the euphotic layer to the Chl *a* concentration within the layer (Morel, 1988). The term Kd_w (λ) denotes attenuation by pure water and Kd_{Bio} (λ) refers to attenuation by all biogenic, optically significant components (algal cells and all associated particulate and dissolved non-algal materials). The following power law function was derived:

$$Kd_{Bio}(\lambda) = \chi(\lambda)[Chla]^{e(\lambda)} \quad (7)$$

Subsequently, the M&M01 model (Morel and Maritorena, 2001) updated the empirical bio-optical model of Kd (λ) using new field data with HPLC determination of Chl *a*, and using a new spectral absorption coefficient of pure water from Pope and Fry (1997). More recently, the BGS07 model extended its applicability into the UV domain and developed a new parameterization based on separated regression analyses for the Mediterranean Sea and South Pacific Ocean (Morel et al., 2007a). In the present work we used these three models to estimate Kd (λ) in the FOD layer (M&M01 and BGS07) and in the euphotic layer (JGR88).

Kd (λ) was computed from T-Chl *a* as follows:

$$Kd(\lambda) = Kd_w(\lambda)+\chi(\lambda)\left[T\_Chla\right]^{e(\lambda)} \quad (8)$$

and

$$Kd_w(\lambda) = a_w(\lambda) + \frac{1}{2}\cdot b_w(\lambda) \quad (9)$$

where χ (λ) and e (λ) were obtained from the models'authors. Mean observed T-Chl *a* profiles in the FOD and the euphotic layers were used as inputs to Eq. (8). For JGR88 and M&M01, Kd_w (λ) was obtained from Morel (1988) and Morel and Maritorena (2001), respectively; for BGS07 it was calculated from Eq. (9). Additionally, empirically derived values of the euphotic depth ($Z_{1\%\text{-Emp}}$) were calculated from the integrated T-Chl *a* concentration (T-Chl a_{Int}) in the euphotic layer, following Morel and Maritorena (2001):

$$Z_{1\%-Emp} = 912.5(T - Chla_{Int})^{-0.839} \quad 10\ m < Z_{1\%-Emp} > 102\ m$$
$$Z_{1\%-Emp} = 426.3(T - Chla_{Int})^{-0..547} \quad 102\ m < Z_{1\%-Emp} > 180\ m \quad (10)$$

2.4.3. Assessments of model performance

Measured values of Kd (λ) were compared with the outputs of the Kirk's and JGR88 models. Either IOP data or T-Chl *a* profiles of the CTD casts within ~2 h of the radiometer casts were used. Modelled values of the broadband Kd (PAR) were calculated by propagating the solar spectrum just below the surface (E_d (λ, 0-)) to a reference depth and numerically integrating over wavelengths following the procedure proposed by Gallegos (1994) and Belzile et al. (2002):

$$Kd(PAR) = -\frac{1}{Z}\cdot Ln\left[\frac{\int_{400}^{700} E_d(\lambda, 0-)\exp[-Kd(\lambda)\cdot Z]d\lambda}{\int_{400}^{700} E_d(\lambda, 0-)d\lambda}\right] \quad (11)$$

where Kd (λ) is the modelled spectral attenuation coefficient, Z is the depth at which PAR is reduced to 1% of its value just below the surface, and E_d (λ, 0-) was solved for each CTD in an iterative manner. Measured values of E_d (λ, 0-) with PRR-800 radiometer were first converted from energy units ($\mu W\ cm^{-2}\ nm^{-1}$) to quantum units ($\mu mol\ photons\ m^{-2}\ s^{-1}\ nm^{-1}$) following Kirk (2011). These were subsequently scaled to the respective measurement of PAR for each optical profiling and then averaged to provide representative E_d (λ, 0-) spectrum per unit of PAR. Following the spectrally-integrated method (Morel, 1988; Gallegos, 1994; Belzile et al., 2002), Eq. (11) was applied to calculate modelled values of Kd (PAR) using the PAR-normalized spectrum to extrapolate the E_d (λ, 0-) for each CTD. Finally, measured values of Kd (PAR) (derived from PRR-800 profiles) were compared with modelled Kd (PAR) values of closer CTDs.

Using modelled Kd (λ) and the extrapolated E_d (λ, 0-) spectra, we constructed the water column light field for each CTD cast by estimating the downwelling component of spectral irradiance at a given depth as follows:

$$E_d(\lambda, Z) = E_d(\lambda, 0-)\exp[-Kd(\lambda).Z] \quad (12)$$

Model performance was assessed by examining the errors between measured and modelled values of Kd (λ, PAR). Statistical tools were the root mean square error (RMSE) and the relative mean error (RME). See below (Section 2.6.) for description.

2.5. Satellite match-up data

Level 3-binned (L3BIN) data from the MODIS-Aqua sensor (daily and 8-day composites, 4.64 km resolution) were matched to in situ measurements using SeaDAS 6.4 ("outtrack" function). We defined the satellite match up as the average value in 3×3 pixel bins. The differences between daily and 8-day composites were minimal. Remote sensing products (2013.1 reprocessing) were obtained from the NASA Ocean Color website (http://oceancolor.gsfc.nasa.gov/), and included Chl*a* concentration (OC3M algorithm; http://oceancolor.gsfc.nasa.gov/cms/atbd/chlora; O'Reilly et al., 1998; see also Morel et al. (2007c)), and the CDOM index (Morel and Gentili, 2009a; product no longer available on the Ocean Color website). The latter expresses the CDOM anomaly with respect to the average CDOM-Chl*a* relationship in Case 1 waters.

2.6. Data and statistical analyses

Given that the main goal of this study was to describe the importance of CDOM in the absorption budget of NW Mediterranean waters, and determine how its contribution to the vertical attenuation coefficient hinders the utilization of Chl *a*-based models of Kd (λ), we primarily analysed both cruises as an entire data set. When differences in optical properties between SU1 and SU2 appeared relevant, the data were analysed separately and conveniently indicated in the text.

Absorption properties and related parameters were analysed and presented separately for three different layers (FOD, DCM and euphotic), for more detailed description and interpretation. Calculations were made from discrete samples collected within the FOD layer 3-8, or 10 m), at the DCM (between 45 and 62 m) and within the euphotic layer (actually between 3 m and the DCM, i.e., slightly narrower than the euphotic layer).

Differences in the mean values of optical properties and derived parameters among water layers, between cruises and between models were tested with One-way ANOVA tests. Simple linear regression and correlation analyses were used to examine the relationships between variables. Prior to each analysis, the Shapiro-Wilk Test and Spearman Rank Correlation were run in order to test for data normality and constant variance, respectively. Whenever the data did not conform, the values were transformed as necessary, or the non-parametric Kruskal-Wallis ANOVA on Ranks was utilized.

To evaluate the performance in the retrieval of Kd (λ, PAR) by the models, the RMSE and RME errors were calculated as follows:

$$RMSE = \sqrt{\frac{\sum_{i=1}^{n}(x_{Mod,i} - x_{Meas,i})^2}{n}} \quad (13)$$

$$RME = \frac{\sum_{i=1}^{n}[(x_{Mod,i} - x_{Meas,i})/x_{Meas,i}]}{n}\cdot 100 \quad (14)$$

where $X_{Mod,\ i}$ and $X_{Meas,\ i}$ are the modelled and measured (observed) values, respectively, and n is the number of data points used.

3. Results

3.1. Oceanographic conditions of the sampling area

The temperature profiles in both cruises depicted MLDs shallower than 10 and 20 m in SU1 and SU2, respectively (Fig. 2). The depth of the euphotic layer ($Z_{1\%}$) was close to 60 m in both cruises, i.e., well below the MLD. In consequence, the waters between 10–20 m and 60 m were sunlit layer and stratified. In both cruises the DCMs were situated within the stratified part of the water column and close to the $Z_{1\%}$ depth (Fig. 2).

The mean T-Chl *a* concentrations in the FOD layer were 0.066 mg m^{-3} in SU1 and 0.078 mg m^{-3} in SU2. At the DCM, the mean T-Chl *a* concentration in SU2 was 1.8 fold higher than in SU1. In the euphotic layer, mean T-Chl *a* was 0.25 ± 0.19 mg m^{-3} in SU1 and 0.36 ± 0.29 mg m^{-3} in SU2. The integrated Chl *a* content in the euphotic layer, T-Chl a_{Int}, was 1.55-fold higher in SU2.

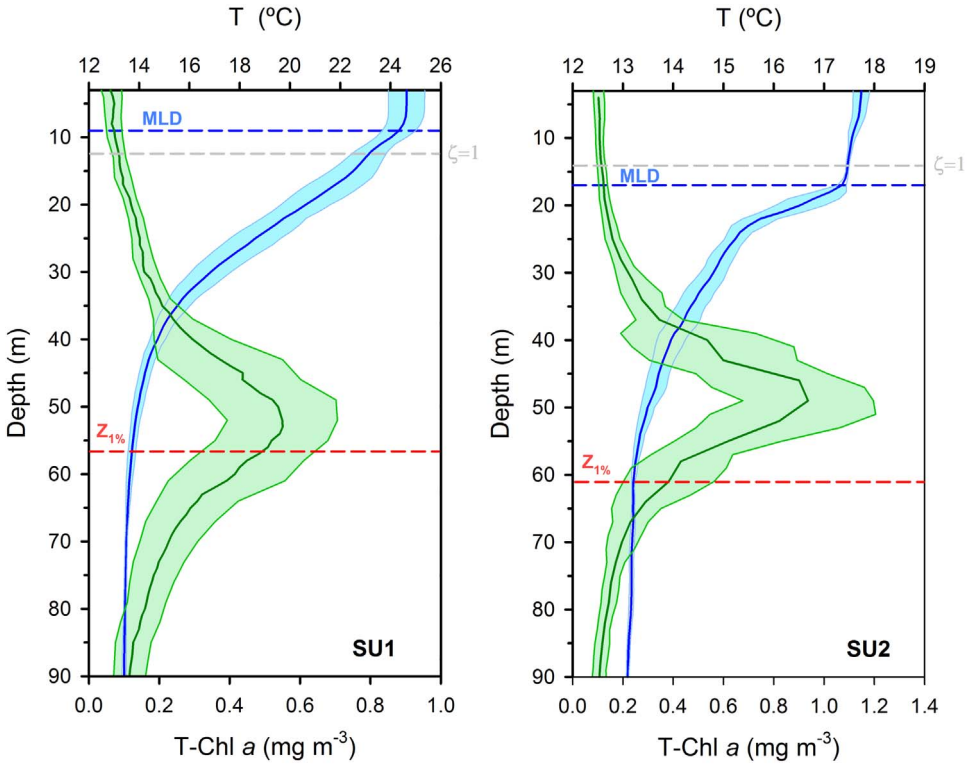

Fig. 2. Vertical profiles of calibrated mean chlorophyll fluorescence (solid green line) and mean temperature (solid blue line) obtained for both cruises. Shaded areas represent ±1 SD. Average values of the first optical depth (FOD; ζ=1), the mixed layer depth (MLD) and the depth of the euphotic layer ($Z_{1\%}$) are indicated with horizontal dashed lines.

3.2. Absorption coefficients of CDOM and particles

3.2.1. Light absorption and spectral features of CDOM

The hypothesis of an unusually high CDOM content per unit of Chl *a* explaining the bio-optical anomaly of the Mediterranean Sea has been investigated before with remote sensing data (Morel and Gentili, 2009a,b) and from CDOM absorption coefficients retrieved by Kd inversion and local determination of particulate absorption (Morel et al., 2007a, 2009). Only a handful of studies have characterized in situ CDOM absorption properties in offshore Mediterranean waters (i.e., Kitidis et al., 2006; Bracchini et al., 2010; Xing et al., 2014; Organelli et al., 2014).

The mean spectral absorption coefficients of CDOM, phytoplankton and non-algal particles measured and calculated in this study are shown in Fig. 3. Within the FOD layer, the mean CDOM absorption coefficients at reference wavelengths 443, 412 and 320 nm were 0.034 ± 0.012, 0.050 ± 0.015 and $0.20 \pm 0.04\ m^{-1}$, respectively. The CDOM absorption between 300 and 590 nm sowed higher values below the FOD layer. For instance, the mean surface a_{cdom} (320) was significant lower than in the rest of the water column (ANOVA, $p < 0.002$) (Fig. 4). In the euphotic layer, the mean values of CDOM absorption coefficients at 443 and 320 nm were $0.043 \pm 0.019\ m^{-1}$ and $0.271 \pm 0.079\ m^{-1}$, respectively.

The spectral slopes of CDOM absorption in the UV region ($S_{275–295}$ and $S_{290–350}$) showed a significant decline between the FOD layer and the DCM (ANOVA, $p < 0.001$). In the FOD layer, the mean $S_{275–295}$ and $S_{290–350}$ were 0.035 ± 0.003 and $0.023 \pm 0.003\ nm^{-1}$, respectively (Table 1). At the DCM, the mean spectral slopes were up to 1.26-fold lower than the surface ones. The other examined spectral slopes ($S_{350–400}$ and $S_{350–500}$) presented rather constant values throughout the water column (Table 1). The spectral metrics ~~[~~S_R and a_{cdom} (250/365)~~]~~ showed the same vertical pattern observed for $S_{275–295}$ and $S_{290–350}$ (Table 1). In the FOD layer, the mean S_R was $2.92 \pm 0.53\ nm^{-1}$ and mean a_{cdom} (250/365) was $18.50 \pm 4.39\ nm^{-1}$. At the DCM a significant decrease in both metrics was observed (ANOVA, $p < 0.001$); with values 1.28 and 1.75-fold lower than at the surface for S_R and a_{cdom} (250/365), respectively.

The FOD-averaged a_{cdom} (443) values reported here were within the range measured by Organelli et al. (2014) at the BOUSSOLE site in the NW Mediterranean Sea (0.012–0.044 m^{-1}). For the same layer, the mean CDOM absorption coefficient at 412 nm was higher than those previously reported by Xing et al. (2014) and Organelli et al. (2014) for the NW basin. In the UV region, however, there was a closer agreement between our surface a_{cdom} observations (e.g., a_{cdom} (300) of $0.34 \pm 0.05\ m^{-1}$) and those reported in previous studies. Organelli et al. (2014) found mean a_{cdom} (300) of 0.35 and 0.41 m^{-1} for November and May, respectively, in the 0–30 m layer. Additionally, Bracchini et al. (2010) reported a_{cdom} (300) values of $0.39 \pm 0.05\ m^{-1}$ in the 0–40 m layer of the central eastern Mediterranean Sea. Comparing to other Case 1 waters, the observed surface mean a_{cdom} (320) in our study was higher than those previously reported by Nelson et al. (2010) for three open ocean basins (a_{cdom} (325) generally $< 0.17\ m^{-1}$).

Comparison of spectral characteristics of FOD CDOM indicate that the values of $S_{350–500}$ reported here ($0.013 \pm 0.002\ nm^{-1}$, Table 1) were lower than those previously reported for the same layer in Mediterranean waters by Organelli et al. (2014) ($0.0175 \pm 0.0015\ nm^{-1}$) and Babin et al. (2003) ($0.017 \pm 0.003\ nm^{-1}$). Spectral slope at shorter wavelengths ($S_{290–350}$) were, instead, very close to those found by Bracchini et al. (2010) ($0.023 \pm 0.003\ nm^{-1}$ vs. $0.025 \pm 0.004\ nm^{-1}$).

Variation of CDOM in the global surface ocean is essentially controlled by the balance between production and degradation processes (Romera-Castillo et al., 2010; De La Fuente et al., 2014), with vertical circulation playing an important role in transporting

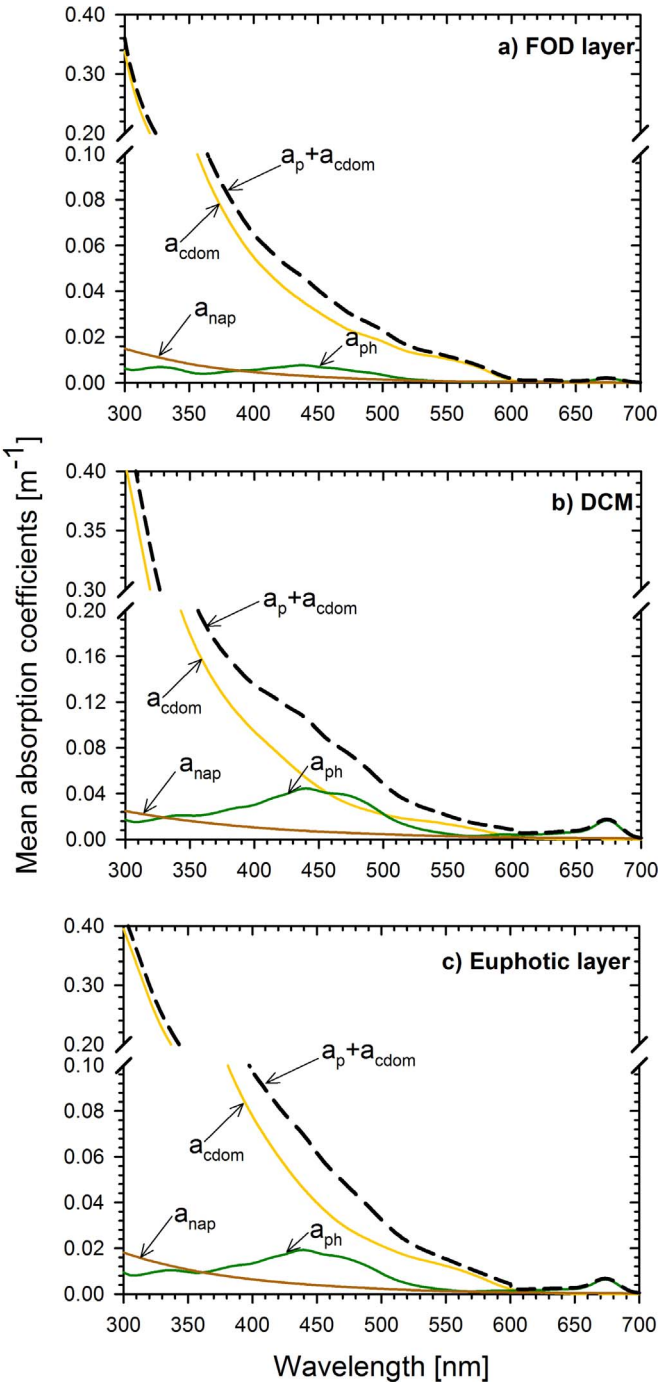

Fig. 3. Spectral absorption coefficients of different optical components within three optically-distinct layers, averaged for the two cruises; a) the FOD layer; b) DCM; and c) the euphotic layer. CDOM is chromophoric dissolved organic matter, p is total particles, pH is phytoplankton and nap is non-algal particles.

CDOM to and from intermediate water masses (Coble, 2007; Nelson and Siegel, 2013). The vertical variation in CDOM observed in the present study, with a subsurface CDOM maximum (hereinafter YSM for Yellow Substance Maximum) (Fig. 4), had already been observed in the Mediterranean Sea. Bracchini et al. (2010) found the a_{cdom} (300) YSM between 40 and 100 m in the eastern basin. In the NW basin, it was found around 50 m during May and September for a_{cdom} (412) (Xing et al., 2014), around 30 m during May through June and 50 m during September through December for a_{cdom} (440) (Organelli et al., 2014), or near 25 m in October for a_{cdom} (412) (Oubelkheir et al., 2005).

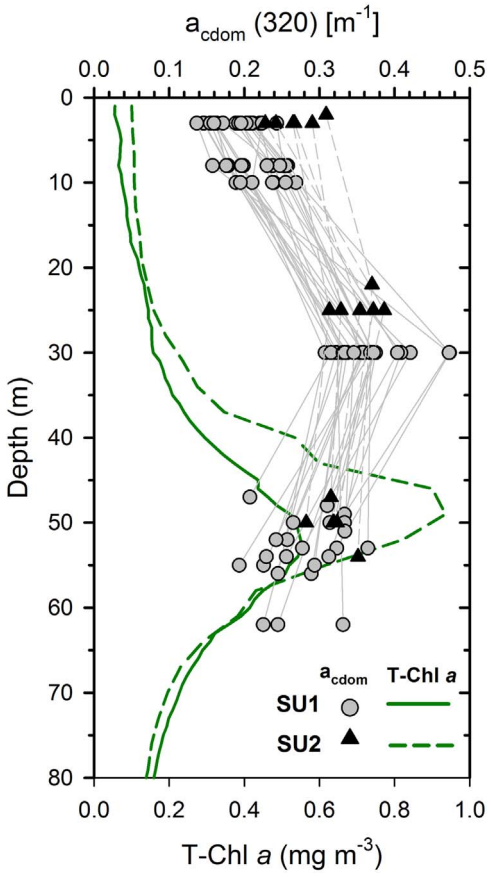

Fig. 4. Vertical variation of a_{cdom} (320) and T-Chl *a* in the SU1 and SU2 cruises.

Organelli et al. (2014) and Xing et al. (2014) discussed the decoupling between the surface and subsurface CDOM dynamics in the Mediterranean and related the observed vertical and seasonal patterns to those of potential drivers. Surface CDOM variation was suggested to be related to physical processes (sea surface temperature and photobleaching), while subsurface CDOM showed tighter coupling with phytoplankton via microbial activity and food web interactions. Our vertical profiles of CDOM features partly support these suggestions: surface waters showed significantly lower absorption coefficients and higher values of $S_{290–350}$, $S_{275–295}$, R_s and a_{cdom} (250/365) than DCM waters. Photobleaching at surface transforms dissolved compounds of high molecular weight into low molecular weight molecules that absorb light at shorter spectral domains, resulting in an increase of slopes and absorption ratios in this spectral region (Twardowski et al., 2004; Helms et al., 2008). Interestingly, in our study this vertical differentiation was not seen at longer wavelengths (i.e., $S_{350–500}$ and $S_{350–400}$). This confirms recent studies that suggest that differences in CDOM optical properties are more evident when the intervals of spectral slopes are limited to the UV wavelengths (Helms et al., 2008; Loiselle et al., 2009; Bracchini et al., 2010). As for the subsurface maximum of CDOM (YSM), hints to its biogenic origin were found in the fact that 30–35 m was the depth of maximum oxygen concentration in the two cruises, according to the O_2 sensor of the CTD (data not shown). All in all, our results on surface CDOM characteristics and their vertical distribution were in good agreement with the few previous studies carried out in the Mediterranean Sea. They all point out that remote sensing of surface properties can hardly depict CDOM dynamics across the entire euphotic layer.

Table 1
Spectral characteristics of CDOM in the three evaluated layers.

	$S_{275-295}$ [nm^{-1}]	$S_{290-350}$ [nm^{-1}]	$S_{350-400}$ [nm^{-1}]	$S_{350-500}$ [nm^{-1}]	S_R	a_{cdom} (250/365)
FOD	0.035 ± 0.003	0.023 ± 0.003	0.015 ± 0.002	0.013 ± 0.002	2.922 ± 0.530	18.502 ± 4.392
DCM	0.030 ± 0.002	0.019 ± 0.002	0.013 ± 0.002	0.015 ± 0.004	2.254 ± 0.287	10.654 ± 2.120
Euphotic	0.033 ± 0.005	0.020 ± 0.002	0.014 ± 0.002	0.014 ± 0.003	2.381 ± 0.601	13.651 ± 4.832

Figures are mean ± 1 SD values pooled from both cruises (SU1 and SU2 as an entire data set) and analysed separately for three layers.

3.2.2. Light absorption by phytoplankton and non-algal particles

The spectral absorption coefficients of phytoplankton (a_{ph}) and non-algal particles (a_{nap}) are shown in Fig. 3. In the FOD layer, the mean values of a_{ph} (443) and a_{ph} (675), corresponding to the blue and red absorption bands of Chl *a*, were 0.007 ± 0.003 and $0.002 \pm 9\ 10^{-4}$ m^{-1}, respectively. Values 5.5 and 8-fold higher (0.043 ± 0.020 and 0.016 ± 0.009 m^{-1}) were recorded at the DCM, following differences in T-Chl*a* concentration. In the euphotic layer, the mean a_{ph} (443) and a_{ph} (675) were 0.022 ± 0.020 and 0.007 ± 0.006 m^{-1}, respectively.

Average a_{nap} (443) was always significantly lower (ANOVA, $p < 0.001$) than the phytoplankton absorption coefficients (Fig. 3). Even though a_{nap} (443) covaried with a_{ph} (443) ($R=0.83$; $p < 0.001$), their relative proportions showed a vertical pattern (data not shown). In the FOD layer, the mean a_{ph} (443) was 2.7-fold higher than a_{nap}(443), whereas this proportion increased to 6.3-fold at the DCM.

The observed values of a_{ph} and a_{nap} are within the previously reported variation of phytoplankton and non-algal particles in the Mediterranean Sea (Bricaud et al., 1998, 2004; Loisel et al., 2011). For instance, surface a_{ph} (440) and a_{ph} (675) observed during the PROSOPE cruise across the two Mediterranean basins in September, ranged roughly 0.003–0.02 m^{-1} and 0.001–0.006 m^{-1}, respectively (Bricaud et al., 2004). Also across the entire Mediterranean but in summer, non-algal particle absorption a_{nap} (440) ranged from 0.0017 to 0.0058 m^{-1} between the surface and the DCM (Loisel et al., 2011). The proportions between the two main particulate constituents reported here are also consistent with Loisel et al. (2011), yet a higher contribution by non-algal particles (a_{nap} (440)/a_p (440) up to 0.8) was observed by Bricaud et al. (1998).

3.2.3. Absorption budget

The relative contributions of CDOM, phytoplankton and non-algal particles to non-water total spectral absorption, i.e., ai (λ)/(a_t (λ)-a_w (λ)) are shown in Fig. 5. For wavelengths smaller than ~600 nm, CDOM was by far the largest contributor in the FOD layer (Fig. 5(a)).

It accounted for > 90% of total non-water absorption at 300 nm and around 80% at 443 nm. Noticeably, CDOM dominated absorption not only in the UV and blue but also in the blue-green spectral region. The remaining components made a much smaller contribution to the total non-water absorption budget in the FOD layer: e.g., a_{ph} (443) contributed ca. 20% and a_{nap} (443) contributed < 7%. At the DCM, the phytoplankton a_{ph} (443) contribution increased to 42%, for ca. 50% accounted for by a_{cdom} (443) (Fig. 5(b)). When averaged over the entire euphotic layer, CDOM clearly dominated non-water absorption (Fig. 5(c)).

Based on the absorption budget, the waters surveyed in this study can be classified as "CDOM-type". In the ternary plot of the optical classification of natural waters using absorption at 443 nm, our samples of the FOD layer were located close to the CDOM apex (Fig. 6). Prieur and Sathyendranath (1981) proposed this triangular classification of natural waters using an absorption budget derived from a statistical analysis of Kd and reflectance.

In contrast to our observations, these authors found that light

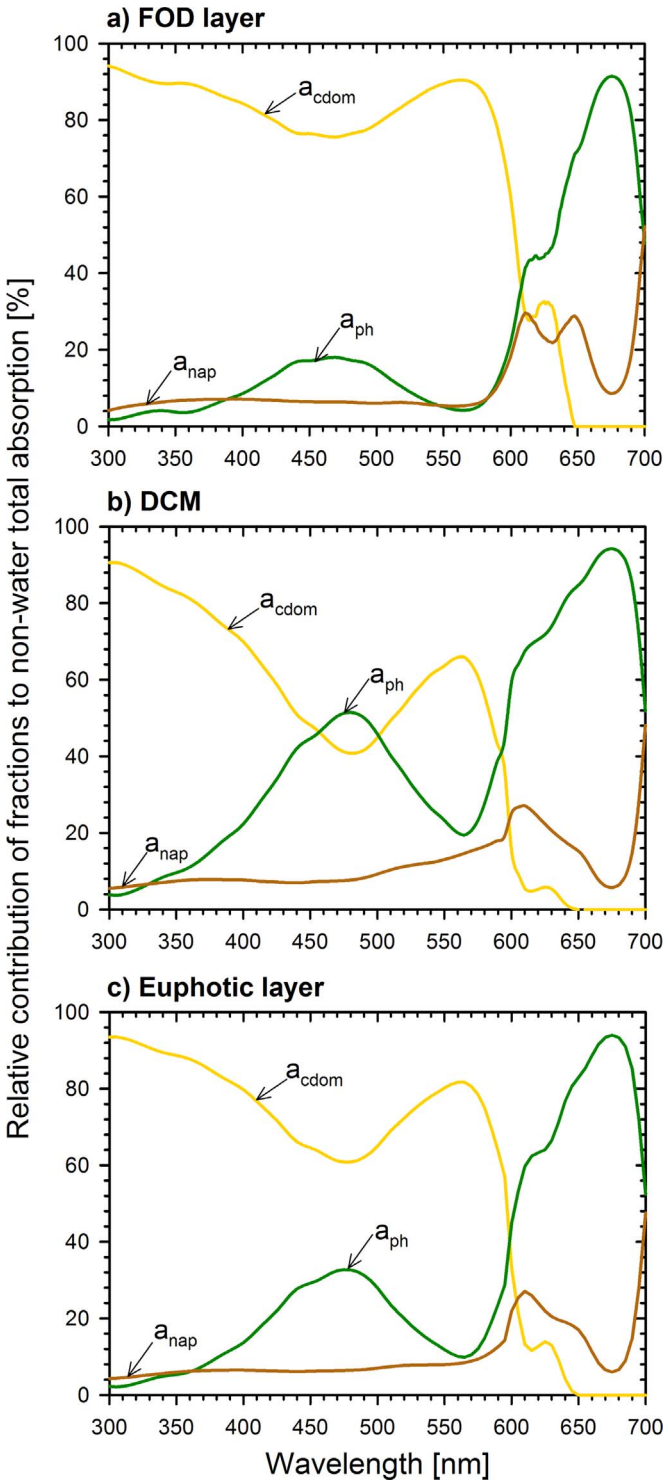

Fig. 5. Mean relative contribution of different absorbing components to total non-water absorption spectra pooled for both cruises in: a) the FOD layer; b) DCM and c) the euphotic layer.

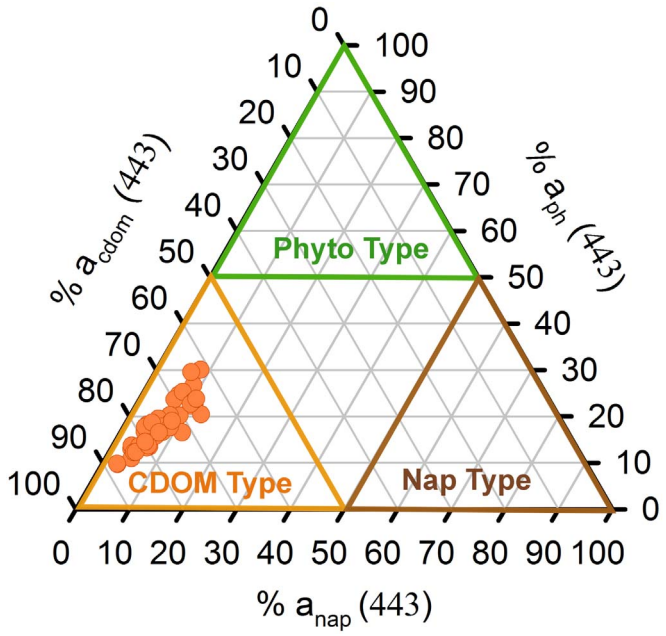

Fig. 6. Ternary plot showing the relative contribution of different absorbing components to total non-water absorption spectra at 443 nm. The data set for the FOD layer of both SUMMER cruises (n=47). Presented as coloured lines, the boundaries of the optical classification for different types of water following Prieur and Sathyendranath (1981).

absorption at 440 nm in the open ocean was typically dominated by phytoplankton absorption, which systematically situated samples near to the phytoplankton apex of the ternary plot. Their classification concept was farther extended by IOCCG (2000), proposing that Case 1 waters should typically be found close to the phytoplankton apex, while Case 2 waters could be found anywhere else in the plot. This classification would suggest that Mediterranean waters are Case 2 waters. However, as already stated by Organelli et al. (2014), CDOM in offshore Mediterranean waters originates mainly from local biological processes and its concentration is related to phytoplankton even though the spatial and temporal scales involved in the genesis of phytoplanktonic-based products and their degradation processes may result in temporal uncoupling between CDOM and algal biomass (Bricaud et al., 1981; Morel and Gentili, 2009a; Xing et al., 2014; Organelli et al., 2014; Yuan et al., 2016). Therefore, following a biogeochemical definition (Morel and Prieur, 1977; Antoine et al., 2014), the waters studied here must be considered as Case 1.

The absorption budget reported here clearly denotes the unusual contribution of CDOM to the absorption process of UV and visible radiation in NW Mediterranean waters, as already pointed out by Organelli et al. (2014). In South Pacific waters, for instance, phytoplankton, CDOM and non-algal particles contributed 30–60%, 40–50% and 10–20% to non-water absorption all throughout from surface to the DCM (Bricaud et al., 2010). At the global scale, remote sensing of the FOD layer showed dominance of coloured detrital and dissolved materials (CDM) in the blue band, with CDOM not contributing more than 40% of absorption (Siegel et al., 2002). This global figure has been revised to nearly 50% of the total light absorption at 400 nm (Nelson and Siegel, 2013). Our results show twice as high a CDOM contribution at 443 nm in Mediterranean waters.

3.2.4. Particle beam attenuation and scattering coefficient

The values of particle beam attenuation in both cruises showed the typical vertical pattern for oligotrophic environments, with an increase from the surface to the euphotic layer depth and a maximum coincident with the DCM. In SU1 we observed also a secondary maximum placed at ca. 25 m depth. Mean C_p (660) at 3 m were $0.042 \pm 0.011\ m^{-1}$ in SU1 and $0.082 \pm 0.009\ m^{-1}$ in SU2, with an average of the two cruises of $0.05 \pm 0.02\ m^{-1}$. At the DCM, C_p (660) were $0.10 \pm 0.04\ m^{-1}$ for SU1 and $0.22 \pm 0.04\ m^{-1}$ for SU2, with an average of $0.12 \pm 0.06\ m^{-1}$. SU2 showed significantly higher values of C_p (660) than SU1 (ANOVA, $p < 0.001$). Since particulate and CDOM absorption coefficient were small compared to scattering (~10% of C_p (660) at all stations), the particulate scattering coefficient at 660 nm was slightly lower than C_p (660). The values and vertical patterns of particulate beam attenuation observed in this study are in good agreement with previous studies conducted in Mediterranean waters (Loisel et al., 2011) and in other oligotrophic marine environments (Behrenfeld and Boss, 2003, 2006).

3.3. Diffuse attenuation within the visible and near-UV spectral domains

3.3.1. Measured values of Kd (λ) in the FOD and euphotic layer

The mean values of measured Kd (443) and Kd (490) in the FOD layer were 0.043 ± 0.004 and $0.039 \pm 0.005\ m^{-1}$, respectively. In the red region, the mean Kd (670) amounted to $0.47 \pm 0.04\ m^{-1}$. In the UV spectral domain, the mean Kd (320) was $0.23 \pm 0.01\ m^{-1}$ (Table 2). Over the euphotic layer, measured Kd (490), Kd (320) and Kd (PAR) values were 0.058 ± 0.003, 0.36 ± 0.04 and $0.079 \pm 0.006\ m^{-1}$, respectively (Supplementary Table S1).

All these measurements were comparable with previous determinations in Mediterranean waters. For instance, Morel et al., (2007a) reported values of FOD Kd (440) and Kd (320) that varied from about 0.03–0.3 m^{-1} and 0.1–0.5 m^{-1}, respectively. Morán and Estrada (2005) determined values of $Z_{1\%}$ ranging from 45 and 68 m in deep offshore sampling stations, representing Kd (PAR) values ranging between 0.068 and 0.098 m^{-1}. Similar attenuation coefficients have been measured in other oligotrophic open ocean regions: Wang et al. (2008) reported FOD Kd (490) values of 0.032 m^{-1} in the Northern South China Sea, and Morel et al., (2007a) reported Kd (320) varying from about 0.05–0.5 m^{-1} in the South East Pacific. Conversely, lower Kd (λ) are often observed: FOD Kd (490) routinely derived from remote sensing measurements were about 0.023 m^{-1} in the Sargasso Sea (Six et al., 2007), and low values of euphotic layer Kd (PAR) are also common in the Sargasso Sea (Tyler, 1975; Smith et al., 1989) and in the North Pacific (Bienfang et al., 1984).

Figures as in Table 2. For the JGR88 model, the values of $Kd_w(\lambda)$ were obtained from Morel (1988). Figures for PAR denote the broad band Kd (PAR). In both models (Kirk´s and JGR88) the values of Kd (PAR) were resolved by the spectrally-integrated method (see Section 2.4.3). Figures for $Z_{1\%}$ denote the euphotic depth calculated from measured and modelled Kd(PAR).

3.3.2. Optical modelling of spectral light attenuation: contribution of different components

To the best of our knowledge, no previous study have assessed the contribution of absorption and scattering to downwelling irradiance diffuse attenuation supported by in situ measurements of CDOM and particulate optical properties in Mediterranean waters.

Kd (λ) computed with Kirk's model showed good general agreement with measured values for both the FOD and euphotic layers (Fig. 7(a) and (b)). In the spectral region 380–490 nm, the model slightly overestimated Kd (λ) in the FOD layer (Table 2, Fig. 7(a)) and performed better for the overall euphotic layer (Supplementary Table S1, Fig. 7(b)). For wavelengths > 600 nm, conversely, the model tended to overestimate Kd (λ) in the euphotic layer (Supplementary Table S1). This differential

Table 2
Measured and modelled Kd (λ) for the FOD layer at several reference wavelengths and the quantification of model performance by the RMSE and RME errors.

λ	Measured	Kirk's Model			M&M01 Model			BGS07 Model		
	Kd_{mea} [m^{-1}]	Kd_{mod} [m^{-1}]	RMSE	RME %	Kd_{mod} [m^{-1}]	RMSE	RME %	Kd_{mod} [m^{-1}]	RMSE	RME %
320	0.226 ± 0.011 (0.202–0.243)	0.238 ± 0.036 (0.197–0.289)	0.032	11.90				0.168 ± 0.014 (0.140–0.186)	0.059	25.77
340	0.141 ± 0.008 (0.124–0.155)	0.161 ± 0.029 (0.126–0.206)	0.031	17.80				0.118 ± 0.012 (0.095–0.132)	0.025	16.51
380	0.085 ± 0.005 (0.074–0.093)	0.097 ± 0.021 (0.070–0.125)	0.023	24.75	0.035 ± 0.004 (0.027–0.041)	0.050	58.81	0.063 ± 0.008 (0.049–0.722)	0.022	25.90
412	0.053 ± 0.003 (0.046–0.058)	0.068 ± 0.011 (0.053–0.085)	0.014	27.69	0.029 ± 0.004 (0.021–0.035)	0.025	45.50	0.040 ± 0.006 (0.029–0.048)	0.014	24.10
443	0.043 ± 0.004 (0.035–0.047)	0.055 ± 0.008 (0.044–0.064)	0.014	28.52	0.027 ± 0.004 (0.020–0.032)	0.017	37.43	0.033 ± 0.005 (0.024–0.039)	0.011	22.84
490	0.039 ± 0.005 (0.028–0.047)	0.044 ± 0.008 (0.034–0.060)	0.011	24.47	0.028 ± 0.003 (0.023–0.031)	0.012	27.96	0.034 ± 0.004 (0.028–0.039)	0.008	14.77
555	0.083 ± 0.008 (0.068–0.094)	0.074 ± 0.005 (0.062–0.079)	0.014	13.58	0.067 ± 0.002 (0.065–0.069)	0.017	17.76	0.076 ± 0.003 (0.072–0.080)	0.010	9.13
670	0.467 ± 0.041 (0.402–0.549)	0.444 ± 0.001 (0.442–0.446)	0.045	7.25	0.447 ± 0.002 (0.443–0.449)	0.043	6.79			

Figures are mean ± 1 SD values and range. Measured and modelled Kd (λ) values for the FOD layer were obtained in both cruises (SU1 and SU2 and as an entire data set). For the M&M01 model, the values of Kd_w(λ) were obtained from Morel and Maritorena (2001), and in the BGS07 model Kd_w (λ) was calculated from Eq. (9) (see Section 2.4.2.).

performance of the model across the light spectrum and depth can be explained by the depression of measured Kd (λ) at longer wavelengths due to the replacement of downwelling irradiance by the inelastically scattered radiation (the Raman emission) and, within a narrower band, by the emission of Chl *a* fluorescence (Morel and Maritorena, 2001). These effects are not considered by the Kirk's model, which is only based on the main IOPs (absorption and scattering coefficients), the angular distribution of photons, and the volume scattering function (Kirk, 2011).

The modelled Kd(PAR) for the euphotic layer, obtained by the spectrally-integrated method (see Section 2.4.3), had a mean value of 0.091 ± 0.009 m^{-1}, 1.15-fold higher than the measured Kd (PAR) (RMSE and RME values of 0.016% and 17%, respectively) (Supplementary Table S1). If only SU1 is considered for data analysis (details not shown), a closer mean value is obtained with the model (0.088 ± 0.004 m^{-1}), only 1.11-fold higher than the average measurement (with RMSE and RME values of 0.009% and 11%, respectively). The modelled mean depth of the euphotic layer for both cruises ($Z_{1\%}$ = 51.12 ± 3.21 m), derived from modelled Kd (PAR), was 7 m shallower than the measured $Z_{1\%}$ (58.32 ± 4.21 m) (Supplementary Table S1). The difference decreases to 5 m if only the SU1 data set is considered.

Optical modelling of Kd (λ) could be improved either by taking discrete samples at smaller depth intervals (e.g. every 10 m, or every 1 m within the FOD layer) or by measuring continuous IOP vertical profiles with absorption and beam attenuation metres (e.g., Simon and Shanmugam, 2013; Boss et al., 2013). Improving measurements of CDOM with Liquid waveguide capillary cells

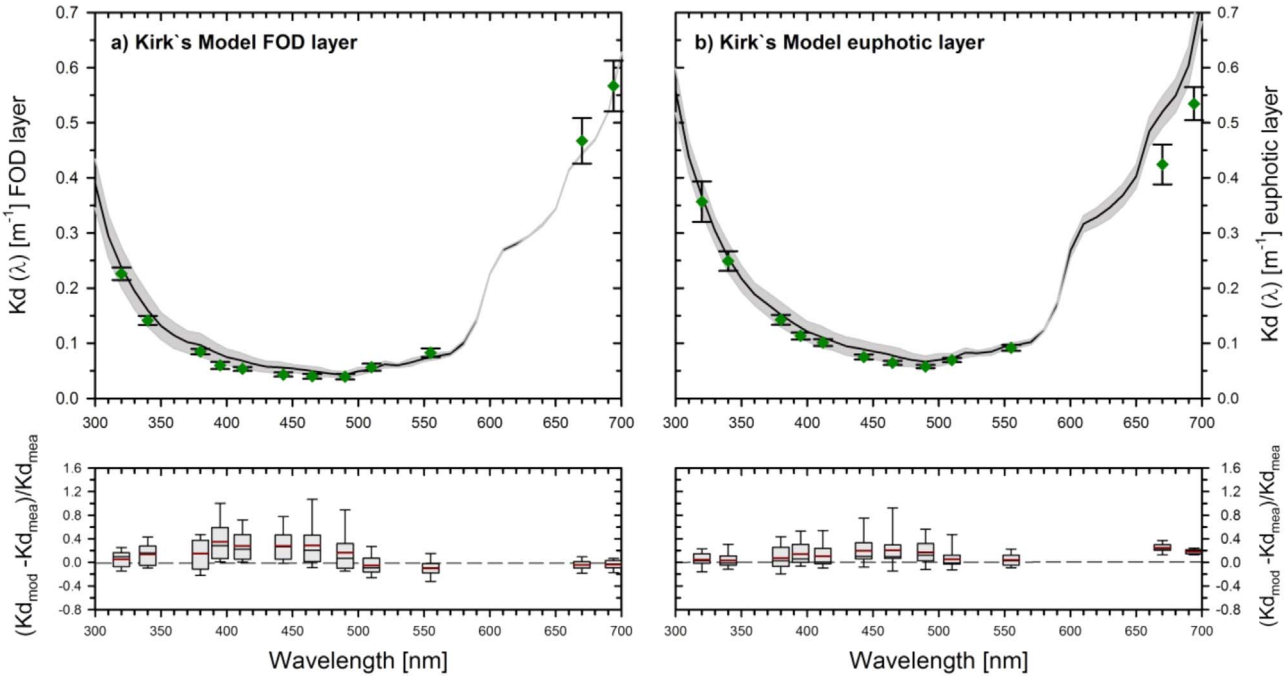

Fig. 7. Mean Kd (λ) measured and modelled with Kirk's optical model applied to both cruises and for: a) the FOD layer and b) the euphotic layer. In the upper panels: green circles show averages of measured Kd at 12 reference wavelengths in the 320–700 nm range; black line shows modelled Kd (λ). Bars and shaded areas indicate ± 1 SD. In the lower panels: box plots display differences between measured and modelled Kd (λ). Bars indicate 25 and 75 percentiles. The black and red lines within the box represent the median and mean values, respectively. (For interpretation of the references to color in this figure legend, the reader is referred to the web version of this article.)

(e.g., D'Sa et al., 1999; Miller et al., 2002; Nelson and Siegel, 2013) and high sensitive point-source integrating-cavity absorption meter (Röttgers and Doerffer, 2007), would also be important to upgrade optical modelling of diffuse light attenuation in Case 1 waters.

Given that the SU2 cruise added much variance in the optical modelling of Kd (λ), and had coarser vertical resolution of discrete measurements (3 depths vs. 4 depths in SU1), only the SU1 data set was considered to calculate the relative contributions of main IOPs (absorptions and particle scattering) to irradiance attenuation. Contributions were calculated following procedures set forth by Belzile et al., (2002) (see Section 2.4.1.). Between 320 and 555 nm, CDOM absorption dominated by >50% the non-water diffuse attenuation coefficient, Kd_{Bio}, in both the FOD and euphotic layers (Fig. 8(a) and (b)). In the FOD layer, CDOM contributed 78% and 72% of Kd_{Bio} at 412 and 443 nm, respectively. In both layers, CDOM contributed ca. 90% of non-water UV attenuation at 320 nm (Fig. 8(a) and (b)). The contribution of phytoplankton absorption was higher for the euphotic layer, and maximal (25%) in the blue spectral band (443–490 nm) and around 52% at 675 nm (Fig. 8(b)).

Absorption by non-algal particles had a minor (<10%) contribution uniformly distributed over the light spectrum. The contribution of particle scattering showed a steady increase from 320 to 625 nm (Fig. 8(a) and (b)), with maximal shares at 625 nm (>75%) and at the red end of the spectra (>85%).

Again, comparison of our results with other Case 1 waters highlighted the importance of CDOM in the irradiance attenuation process of the Mediterranean Sea. For instance, Siegel and Mitchaels (1996) reported that CDM and phytoplankton contributed equally to Kd (440) in the Sargasso Sea. Following Nelson et al. (1998), the contribution of different components to irradiance diffuse attenuation can alternatively be assessed as the ratio between Kd and the absorption coefficient of interest. With this approach, the CDOM contribution to Kd (320) in our study was 2-4-fold higher than that estimated for the South Pacific gyre using the Kd and a_{cdom} (310 nm) data reported by Morel et al. (2007b).

3.3.3. *Chl a-based models of diffuse attenuation coefficients*

3.3.3.1. The FOD layer. The M&M01 bio-optical model (Morel and Maritorena, 2001) has been widely applied to estimate AOPs (i.e., Kd (λ) and R (λ)) and derived parameters (i.e., $Z_{1\%}$) from Chl *a* concentration in Case 1 waters.

With our dataset from both cruises, the M&M01 model largely underestimated FOD Kd (λ) in the 380–555 nm range (Fig. 9(a)). The discrepancy to measurements increased towards shorter wavelengths, further evidencing the effect of the contribution of CDOM absorption to irradiance attenuation. Values of RMSE and RME at 380 nm were 0.050% and 59%, respectively, and decreased to a minimum between 555 and 670 nm (0.04% and 18%) (Table 2).

The outcome of the regionally tuned (for the Mediterranean) BGS07 model matched Kd (λ) measurements much better than the global M&M01 model (Fig. 9(b)), particularly in the 412–555 nm band, where RMSE and RME were lower than 0.014% and 24%, respectively (Table 2). In the UV domain (320 and 380 nm), however, BGS07 also underestimated Kd (RMSE and RME up to 0.059% and 26%, respectively).

It is worth noting that the Chl *a*-based models of Kd (λ) assessed here have a "static" condition, i.e., they are insensitive to daily and vertical variations in the three-dimensional light field. This simplification contributes to make these Chl *a*-based models the most widely used by the community (e.g., Mitchell and Holm-Hansen, 1991; Bricaud et al., 2004; Lee et al., 2005; Uitz et al., 2006; Suresh et al., 2012; Organelli et al., 2014). However, Morel and Gentili (2004) modelled the effects of solar zenith angle and other external conditions on Kd (λ) and reported an increase of 35–45% when the solar angle varies from 0° to 75°, independently of wavelength. Our measurements of downwelling irradiance were carried out at solar zenith angles varying between 24° and 54°. Therefore, differences in solar elevation should not, by themselves, explain the observed differences between measured and modelled Kd (λ). Moreover, both models showed an increase in the underestimation of Kd (λ) with decreasing wavelengths; this can hardly be associated with differences in solar angle, but with the effect of CDOM absorption.

Using the equation proposed by Xing et al., (2012) (their Eq. (9)), we were able to decompose the modelled Kd_{Bio} (412) using Chl *a*-based models with the purpose to estimate the contribution of CDOM absorption to the diffuse attenuation in the FOD layer. In M&M01, CDOM absorption contributed ca. 52% of diffuse light attenuation, a figure that increased to 70% in BGS07. These percentages are 1.5 and 1.1-fold lower respectively than the values estimated with Kirk´s model (see Fig. 8).

The observed differences between BGS07 modelled and measured Kd (λ) could be related to the natural variation (spatial and temporal) of bio-optical properties in the Mediterranean Sea. In fact, BGS07 was developed using the average Kd (λ) vs. Chl *a* relationship found in the FOD layer for the two Mediterranean

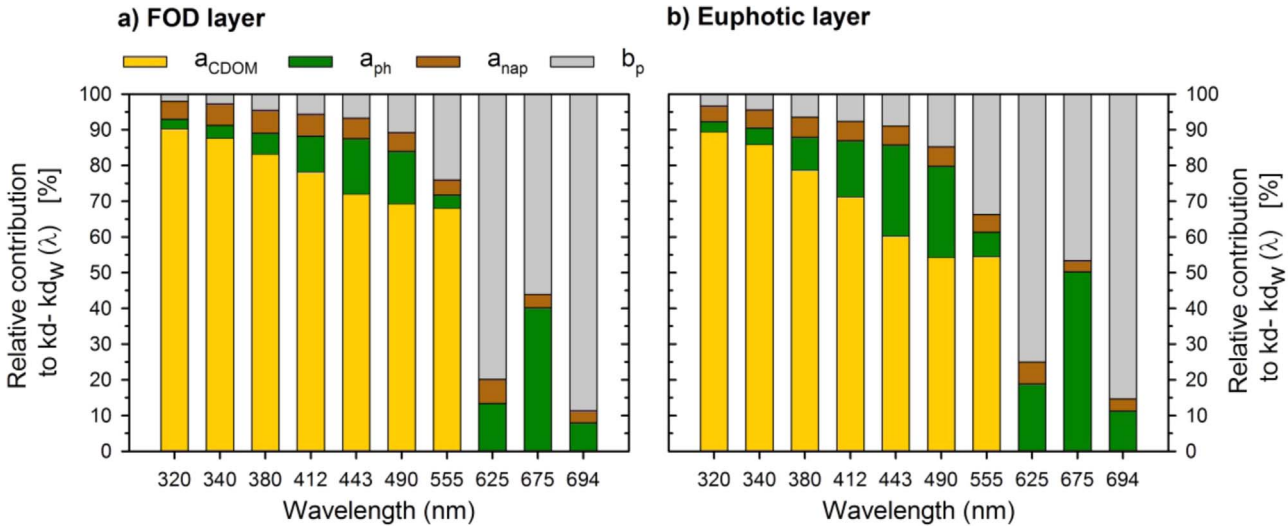

Fig. 8. Contribution of IOPs to Kd_{Bio} (=Kd-Kd_w) at several reference wavelengths in a) the FOD layer, and b) the euphotic layer.

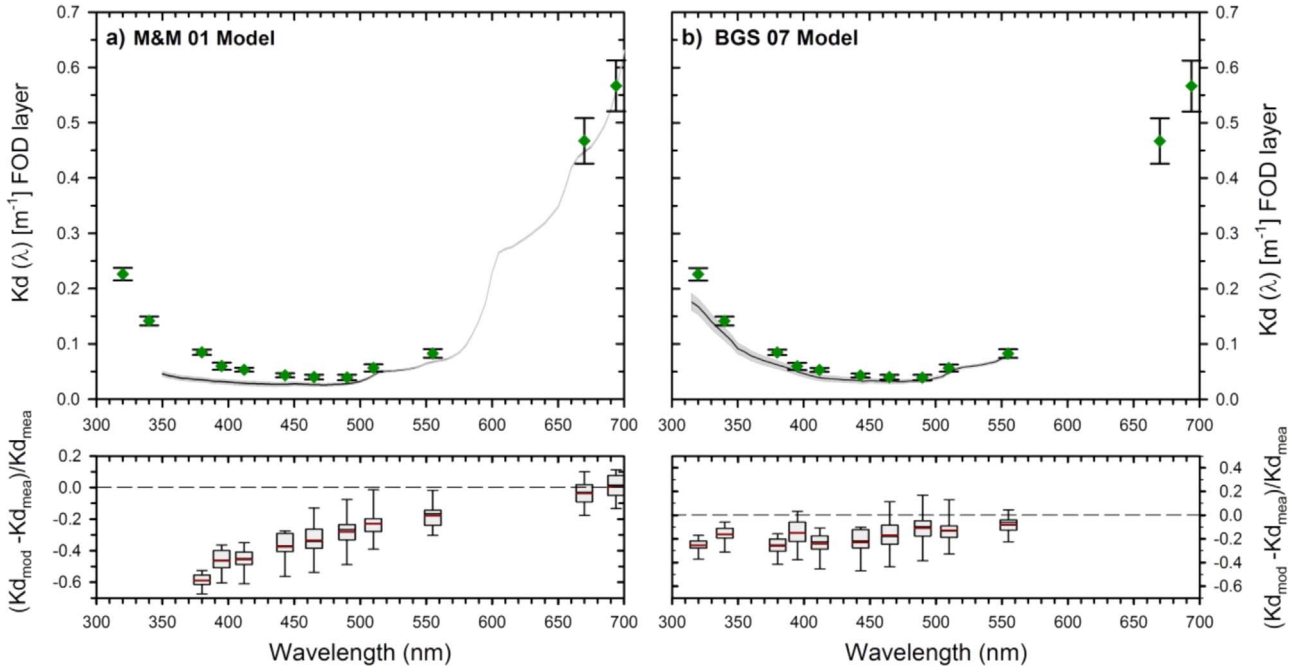

Fig. 9. Mean FOD values of Kd (λ) measured and modelled with Chl *a*-based models for both cruises. As in Fig. 7, but for: a) Kd (λ) modelled with M&M01 model and b) Kd (λ) modelled with BGS07.

basins. Therefore, knowing that the western basin contains higher CDOM per unit Chl *a* than the eastern basin (Morel and Gentili, 2009b; Xing et al., 2014), some underestimation of Kd (λ) with BGS07 was expected in the NW Mediterranean. In addition, the relationship between Chl *a* and CDOM has been shown to change at short time scales (weeks), with a lag of a_{cdom} (443) relative to a_{ph} (443) that varies with seasons (Hu et al., 2006). All in all, misestimates of Kd (λ) with Chl *a*-based models of pretended general applicability are not unexpected.

3.3.3.2. The euphotic layer. The JGR88 model underestimated Kd (λ) specially at 412 and 443 nm in the euphotic layer (Supplementary Fig. S1, Table S1). RMSE and RME at 412 nm were 0.038% and 36.5%, respectively. The disagreement with measurements decreased towards higher wavelengths owing to the handling of longwave downwelling irradiance by the model (Morel, 1988), so that good estimates were obtained in the red spectral region.

Using the spectrally-integrated method we obtained a mean modelled Kd (PAR) of $0.067 \pm 0.006\ m^{-1}$, 1.17-fold lower than the measured Kd (PAR), which resulted in a ~11 m deeper euphotic layer depth (Supplementary Table S1).

The inaccuracies in the Chl *a*-based modelling of Kd (λ) translate into incorrect estimates of spectral irradiance propagation through the euphotic layer. A synthetic view of this problem was presented in Fig. 10. The spectral downwelling irradiance propagation through the euphotic layer was calculated using JGR88 and was then compared with the downwelling irradiance measured at the DCM. JGR88 simulations of Ed (λ, Z) gave too much radiation in the blue (400–460 nm) due to the underestimation of Kd (λ) (see Fig. S1).

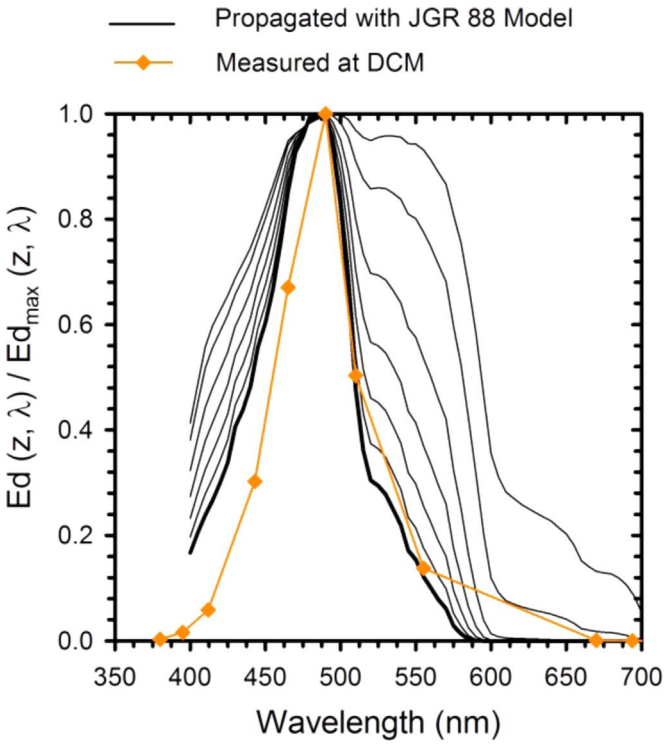

Fig. 10. Example of estimated downward spectral irradiance at various depths (5, 10, 20, 30, 40, 50 m and DCM) for CTD#5 of cruise SU1 at noon, propagated using the JGR88 model. Black lines: modelled Ed(λ); orange line and diamonds: measured Ed(λ) at the DCM. (For interpretation of the references to color in this figure legend, the reader is referred to the web version of this article.)

4. Discussion

Accurate description and prediction of underwater optics is critical in marine ecology and biogeochemistry. Determination of Kd (λ, PAR) and related variables (i.e., $Z_{1\%}$) is essential for aquatic models of primary production, PP, (e.g., Platt et al., 1988; Lee et al., 1996; Behrenfeld and Falkowski, 1997; Falkowski and Raven, 1997). Kd (λ, PAR) is also a key variable for determining heat transfer in the upper ocean (e.g., Lewis et al., 1990; Morel and Antoine, 1994; Chang and Dickey, 2004) and for understanding carbon (Mopper et al., 1991; Moran and Zepp, 1997; Lefèvre et al., 2003), nitrogen (Bushaw et al., 1996; Vähätalo and Zepp, 2005; Aarnos et al., 2012) or sulphur (Vallina and Simó, 2007; Miles

et al., 2009; Galí et al., 2013) biogeochemical processes.

Chl *a*-based modelling of Kd (λ) has often been used to describe the propagation of spectral irradiance through the water column. For instance, the JGR88 model has been used to estimate E_d (λ, Z) for modelling carbon: nitrogen and carbon: Chl*a* ratios (Lefèvre et al., 2003) and for wavelength-resolved models of primary production (PP, Smyth et al., 2005; Tilstone et al., 2005, 2015). Semi-analytical algorithms for PP modelling, that include information on the photophysiology of phytoplankton and the spectral quality of light, such as the effective absorption coefficient (a_{eff}^*), the phytoplankton usable radiation (PUR) and the maximum photosynthetic quantum yield (ϕ_{max}), must take into account the limitations of E_d (λ, Z) calculations based only on Chl *a* parameterization, as pointed out by Smyth et al. (2005) and Tilstone et al. (2005). This was also discussed by Antoine et al. (2013), who used the M&M01 model to determine the percentage of surface spectral irradiance that reaches the DCM in the Beaufort Sea, and highlighted the importance of including CDOM absorption in light propagation models and its consequences for a reliable modelling of net primary production in Arctic waters.

Global empirical relationships between $Z_{1\%}$ and either surface or column integrated T-Chl *a* concentration have previously been

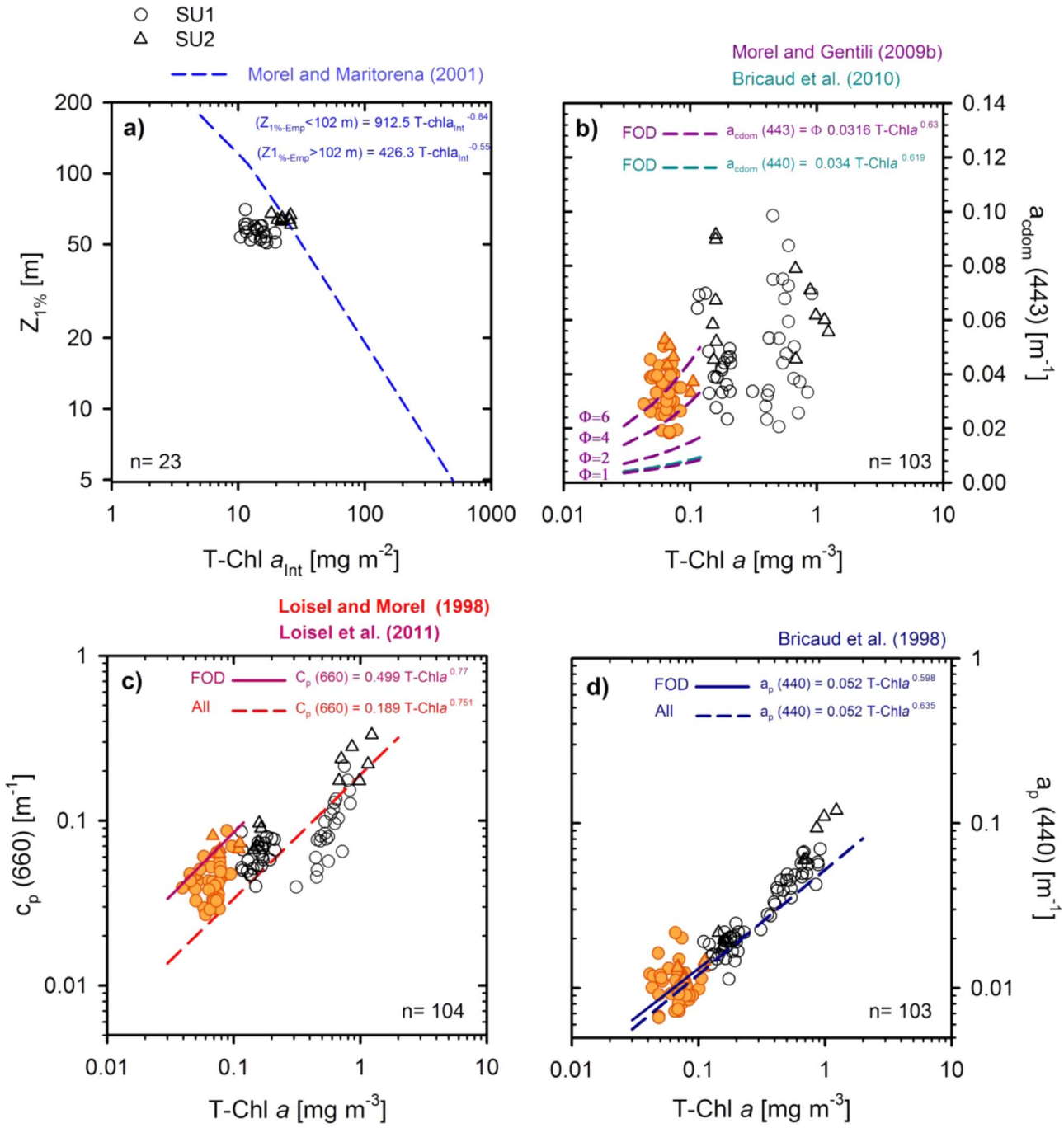

Fig. 11. Bio-optical relationships obtained by pooling all the data set of the SU1 and SU2 cruises. Water samples from the FOD layer are plotted in orange. In a), c) and d) coloured continuous lines, short dashed lines and equations represent average relationships previously reported for Case 1 waters. In b) different CDOM indexes (from 1 to 6) and the relationships previously established for the FOD layer by Morel and Gentili, (2009b) are plotted to obtain an average scaling factor for the present work. The CDOM-Chl *a* relationship established by Bricaud et al. (2010) is also overlaid. (For interpretation of the references to color in this figure legend, the reader is referred to the web version of this article.)

proposed for Case 1 waters (Morel, 1988; Morel and Maritorena, 2001; Morel et al., 2007a,c). Our values of $Z_{1\%}$ were notably lower than those predicted for average Case 1 waters (see blue dashed line in Fig. 11(a)). This further illustrated the strong dimming effect of CDOM absorption in the NW Mediterranean Sea.

The observed mean value of $Z_{1\%}$ (58.32 m $\pm$4.21 m) was 28 m shallower than the mean value predicted by the Morel and Maritorena (2001) empirical relationship ($Z_{1\%\text{-emp}}=86.08\pm14.06$ m) (Eq. (10), see Section 2.4.2). It is worth noting that smaller differences are obtained if the JGR88 model is used to estimate Kd (λ) and then the spectrally-integrated method is applied to obtain Kd (PAR), subsequently used to determine $Z_{1\%}$ (see Section 3.3.3.2 and Supplementary Table S1). Morel (1988) had already pointed out that $Z_{1\%}$ was not adequately predicted as a power law of Chl *a* at very low Chl *a* concentrations. Departures from the average relationship between $Z_{1\%}$ and Chl *a* had formerly been observed in Mediterranean waters (Morel et al., 2007a) as well as in other oceanic regions with high CDOM content. In clear open ocean waters of the Canadian Beaufort Sea, for instance, Antoine et al. (2013) found $Z_{1\%}$ shallower than those predicted using average $Z_{1\%}$-Chl *a* relationship for Case 1 waters.

Within the natural variability of Case 1 waters, CDOM content is one of the important factors governing the optical properties that cannot be explained by the variation in Chl *a* concentration. As expected, in our study CDOM absorption coefficients in the FOD layer were recurrently above the average relationships proposed by Morel and Gentili (2009b) and by Bricaud et al. (2010) for Case 1 waters (Fig. 11(b)). The factor Φ ("CDOM index") was introduced by Morel and Gentili, (2009a) to account for the variability around the average CDOM-Chl *a* relationship established for the upper layer of Case 1 waters. The average relationship is represented by the equation in Fig. 11(b) when $\Phi=1$; a factor $\Phi>1$ or <1 indicates "excess" or "deficit" of CDOM compared to the average Case 1 value for a given Chl *a* content. In the FOD layer of our cruises, the mean measured a_{cdom} (443) and T-Chl *a* yielded a $\Phi=5.9$. This is higher than values previously reported for W Mediterranean waters using remote sensing data with Φ varying between about 2.5-5.5 (Morel and Gentili, 2009b). These authors observed a notable seasonal variation in Φ, with average values around 4 in May and around 2.5 in September.

The anomalously high absorption coefficients per unit of T-Chl *a* observed from our measurements at sea were consistent with simultaneous remote sensing estimations by MODIS. Although lower than values obtained in situ, mean Φ values derived from MODIS ($\Phi=4.6\pm0.5$ for SU1 and $\Phi=5.1\pm0.4$ for SU2, average $\Phi=4.8\pm0.4$) were also higher than mean values previously reported for NW Mediterranean waters in May and September. As expected, MODIS Chl *a* concentrations were 2-fold higher than those experimentally determined by HPLC. If we use MODIS estimates of Φ to recalculate the CDOM contribution to diffuse attenuation coefficient using the Kirk's model (see Section 2.4.1.), we obtain that CDOM contributed 74% and 65% to Kd_{Bio} at 412 and 443 nm, respectively, in the FOD layer. These values are close to those obtained with Kirk's model using in situ CDOM measurements (Fig. 8(a)) and intermediate between the latter and those obtained with the BGS07 model (Section 3.3.2.).

We cannot rule out a moderate overestimation of absorption coefficients at the low CDOM concentrations observed in the FOD, due to light dispersion by small particles remaining in the sample after filtration (Röttgers and Doerffer, 2007). This potential overestimation could explain inaccuracies in the optical modelling of Kd (λ) in the FOD layer (Fig. 7(a)) and also differences between MODIS and in situ estimates of Φ. However, this would not change our main outcome of the outstanding role of CDOM in the underwater optical properties of the Mediterranean Sea, supported also by MODIS data and BGS07.

Another factor that we should not rule out when assessing the optical peculiarities of NW Mediterranean waters is the presence of suspended submicron Saharan dust particles. This phenomenon has been suggested as a plausible explanation for concomitant decreases in both the absorption a_t (555)/a_t (440) and the backscattering b_b (440)/b_b (555) ratios, and also for enhancement of b_p (555) (Claustre et al., 2002). Loisel et al. (2011) also observed high particulate beam attenuation and b_{bp}/T-Chl *a* ratios in NW Mediterranean waters. Moreover, higher scattering coefficients could also contribute to enhanced values of Kd (λ) in the region (Morel et al., 2007a). Measured particulate beam attenuation coefficients [c_p (660)] at low, mid and high T-Chl *a* concentrations in this study were above the general empirical mean relationship established by Loisel and Morel (1998) for the euphotic layer of Case 1 waters, and close yet lower than those predicted for the FOD layer (Loisel et al., 2011) (Fig. 11(c)). The c_p (660) is a good proxy of scattering coefficients; therefore, scattering could have also contributed, even if in a lower proportion relative to CDOM absorption, to the light attenuation enhancement relative to Chl *a* concentration in our study.

Finally, the potential irregularity of particle absorption [a_p (440)] relative to T-Chl *a* is worth to explore. Variation of a_p (440) with T-Chl *a* concentration in both cruises (Fig. 11(d)) showed good agreement with the previously reported general relationship for Case 1 waters (Bricaud et al., 1998). The same was observed for phytoplankton absorption at 440 nm (data not shown). Therefore, in the present study, the contribution of particulate absorption to the observed peculiar bio-optics of the Mediterranean Sea was far less important than that of CDOM.

5. Conclusions

Among the possible causes of the observed deviations of bio-optical relationships in the Mediterranean Sea, an unusually high amount of CDOM has frequently been invoked. Nevertheless, only a limited number of studies with in situ determinations of CDOM absorption properties had been conducted in offshore Mediterranean waters. Noticeably, our field study shows that CDOM dominated the total non-water light absorption budget in the first optical depth (FOD) and euphotic layers, not only in the UV and blue, but also in the blue-green spectral region. The CDOM contribution to non-water absorption at 443 nm in the FOD layer was twice the average of global ocean Case 1 waters. As a consequence, CDOM was the largest contributor ($>50\%$) to light diffuse attenuation between 320 and 555 nm across the FOD and the euphotic layers, well above particle absorption and scattering.

The outstanding effects of CDOM in the underwater optical properties of the Mediterranean Sea were further revealed by the application of bio-optical models designed to estimate diffuse attenuation coefficients [Kd(λ)] from Chl *a* concentrations. Measured Kd (λ) in the FOD layer were higher than those predicted by the M&M01 model, which was empirically derived for Case 1 waters of the oligotrophic oceans. The BGS07 model, tuned for the Mediterranean Sea, performed closer to observations. However, it still underestimated Kd (λ) in the UV spectral region, perhaps due to the natural spatial and temporal variation of bio-optical properties that cannot be resolved with two cruises in a particular location. The JGR88 model, developed for the euphotic layer, also underestimated Kd (λ) with respect to observations, with decreasing discrepancy towards longer wavelengths as was also observed for the M&M01 and BGS07 models. Measured euphotic layer depths [$Z_{1\%}$] were on average 28 m shallower than those predicted by empirical relationships for Case 1 waters. Altogether, these model output vs. observation exercises evidenced the large contribution of CDOM absorption (particularly large at shorter wavelengths)

that is not accounted for by the Chl *a* concentration. Indeed, measured CDOM absorption coefficients [a_{cdom} (440)] were notably higher than those expected for the observed T-Chl *a* concentration, and the same held when MODIS-derived data was used instead.

Underwater diffuse irradiance attenuation and related variables like the euphotic layer depth are critical for marine biogeochemical and ecological studies. Inaccuracies of the Chl *a*-based models in the estimation of light attenuation and in the calculation of downwelling irradiance propagation through the euphotic layer, may translate into important errors in the modelling of primary production and biases in the quantification and interpretation of the interactions between plankton or molecules and the spectral composition and intensity of light. Our study calls for caution when applying bio-optical models of general applicability to the optically peculiar waters of the Mediterranean Sea.

Acknowledgments

The authors acknowledge the invaluable assistance and cooperation of the marine technicians (UTM) and the crew aboard R/V Garcia del Cid. This research was funded by the successive Spanish Ministries of Science through projects SUMMER "SUrface Mixing Modulation of the Exposure to solar Radiation" (CTM2008–03309/MAR), PEGASO (CTM2012–37615) and DOREMI (CTM2012–34294), and through the CONICET and CONICET-CSIC scholarships to G. L. Pérez. This is a contribution of the Research Group on Marine Biogeochemistry and Global Change of the ICM, funded by the Catalan Government.

Appendix A. Supporting information

Supplementary data associated with this article can be found in the online version at http://dx.doi.org/10.1016/j.dsr.2016.05.011.

References

Antoine, D., Morel, A., Jean-Michel, A., 1995. Algal pigment distribution and primary production in the eastern Meditteranean as drived from coastal zone color scanner observations. J. Geophys. Res. 100, 16,193–16,209.

Antoine, D., D'Ortenzio, F., Hooker, S.B., Bécu, G., Gentili, B., Tailliez, D., Scott, A.J., 2008. Assessment of uncertainty in the ocean reflectance determined by three satellite ocean color sensors (MERIS, SeaWiFS, and MODIS-A) at an offshore site in the Mediterranean Sea. J. Geophys. Res. 113, C07013, doi:101029/2007JC004472.

Antoine, D., Hooker, S.B., Bélanger, S., Matsuoka, A., Babin, M., 2013. Apparent optical properties of the Canadian Beaufort Sea – Part 1: observational overview and water column relationships. Biogeosciences 10, 4493–4509. http://dx.doi.org/10.5194/bg-10–4493–2013.

Antoine, D., Babin, M., Berthon, J.-F., Bricaud, A., Gentili, B., Loisel, H., Maritorena, S., Stramski, D., 2014. Shedding light on the sea: André Morel's legacy to optical oceanography. Ann. Rev. Mar. Sci. 6, 1–21. http://dx.doi.org/10.1146/annurev-marine-010213–135135.

Aarnos, H., Ylöstalo, P., Vähätalo, A.V., 2012. Seasonal phototransformation of dissolved organic matter to ammonium, dissolved inorganic carbon, and labile substrates supporting bacterial biomass across the Baltic Sea. J. Geophys. Res. 117, 2156–2202. http://dx.doi.org/10.1029/2010JG001633.

Asmala, E., Stedmon, C.A., Thomas, D.N., 2012. Linking CDOM spectral absorption to dissolved organic carbon concentrations and loadings in boreal estuaries. Estuar. Coast. Shelf Sci. 111, 107–117. http://dx.doi.org/10.1016/j.ecss.2012.06.015.

Babin, M., Stramski, D., Ferrari, G.M., Claustre, H., Bricaud, A., Obolensky, G., Hoepffner, N., 2003. Variations in the light absorption coefficients of phytoplankton, nonalgal particles, and dissolved organic matter in coastal waters around Europe. J. Geophys. Res. 108, 1–20. http://dx.doi.org/10.1029/2001JC000882.

Behrenfeld, M., Falkowski, P.G., 1997. A consumer's guide to phytoplankton primary productivity models. Limnol. Oceanogr. 42, 1479–1491. http://dx.doi.org/10.4319/lo.1997.42.7.1479.

Behrenfeld, M.J., Boss, E., 2003. The beam attenuation to chlorophyll ratio: an optical index of phytoplankton physiology in the surface ocean? Deep Sea Res. Part I Oceanogr. Res. Pap. 50, 1537–1549. http://dx.doi.org/10.1016/j.dsr.2003.09.002.

Behrenfeld, M.J., Boss, E., 2006. Beam attenuation and chlorophyll concentration as alternative optical indices of phytoplankton biomass. J. Mar. Res. 64, 431–451. http://dx.doi.org/10.1357/002224006778189563.

Belzile, C., Vincent, W.F., Kumagai, M., 2002. Contribution of absorption and scattering to the attenuation of UV and photosynthetically available radiation in Lake Biwa. Limnol. Oceanogr. 47, 95–107. http://dx.doi.org/10.4319/lo.2002.47.1.0095.

Bienfang, P.K., Szyper, J.P., Noda, E.K., 1984. Temporal and spatial variability of phytoplankton in a subtropical ecosystem. Limnol. Oceanogr. 29, 527–539.

Boss, E., Picheral, M., Leeuw, T., Chase, A., Karsenti, E., Gorsky, G., Taylor, L., Slade, W., Ras, J., Claustre, H., 2013. The characteristics of particulate absorption, scattering and attenuation coefficients in the surface ocean; Contribution of the Tara Oceans expedition. Methods Oceanogr. 7, 52–62. http://dx.doi.org/10.1016/j.mio.2013.11.002.

Bracchini, L., Tognazzi, A., Dattilo, A.M., Decembrini, F., Rossi, C., Loiselle, S.A., 2010. Sensitivity analysis of CDOM spectral slope in artificial and natural samples: an application in the central eastern Mediterranean Basin. Aquat. Sci. 72, 485–498. http://dx.doi.org/10.1007/s00027–010-0150-y.

Bricaud, A., Morel, A., Prieur, L., 1981. Absorption by dissolved organic matter of the sea (yellow substance) in the UV and visible domains. Limnol. Oceanogr. 26, 43–53.

Bricaud, A., Stramski, D., 1990. Spectral absorpion coeffcients of living phytoplankton and nonalgal biogenous matter: A comparision between the Peru upwelling area and the Sargasso Sea. Limnol. Oceanogr 53, 562–582.

Bricaud, A., Babin, M., Morel, A., Claustre, H., 1995. Variability in the chlorophyll-specific absorption coefficients of natural phytoplankton. J. Geophys. Res. 100, 13321–13332.

Bricaud, A., Morel, A., Babin, M., Allali, K., Claustre, H., 1998. Variations of light absorption by suspended particles with chlorophyll a concentration in oceanic (case 1) waters. J. Geophys. Res. 103, 31033–31044.

Bricaud, A., Bosc, E., Antoine, D., 2002. Algal biomass and sea surface temperature in the Mediterranean Basin. Remote Sens. Environ. 81, 163–178. http://dx.doi.org/10.1016/S0034-4257(01)00335-2.

Bricaud, A., Claustre, H., Ras, J., Oubelkheir, K., 2004. Natural variability of phytoplanktonic absorption in oceanic waters: Influence of the size structure of algal populations. J. Geophys. Res. 109, 1–12. http://dx.doi.org/10.1029/2004JC002419.

Bricaud, A., Babin, M., Claustre, H., Ras, J., Tièche, F., 2010. Light absorption properties and absorption budget of Southeast Pacific waters. J. Geophys. Res. 115, C08009. http://dx.doi.org/10.1029/2009JC005517.

Buiteveld, H., 1994. The optical properties of pure water. In: Proceedings of SPIE Oean Opt. XII, 2258, pp. 174–181.

Bushaw, K.L., Zepp, R.G., Tarr, M.A., Schulz-Jander, D., Bourbonniere, R.A., Hodson, R. E., Miller, W.L., Bronk, D.A., Moran, M.A., 1996. Photochemical release of biologically available nitrogen from aquatic dissolved organic matter. Nature 381, 404–407. http://dx.doi.org/10.1038/381404a0.

Chang, G.C., Dickey, T.D., 2004. Coastal ocean optical influences on solar transmission and radiant heating rate. J. Geophys. Res. 109, 1–16. http://dx.doi.org/10.1029/2003JC001821.

Claustre, H., Morel, A., Hooker, S.B., Babin, M., Antoine, D., Oubelkheir, K., Bricaud, A., Leblanc, K., Quéguiner, B., Maritorena, S., 2002. Is desert dust making oligotrophic waters greener ? Geophys. Res. Lett. 29, 10–13.

Claustre, H., Maritorena, S., 2003. The many shades of ocean blue. Sci. York 6, 1514–1515.

Coble, P.G., 2007. Marine optical biogeochemistry: the chemistry of ocean color. Chem. Rev. 107, 402–418.

De La Fuente, P., Marrasé, C., Canepa, A., Antón Álvarez-Salgado, X., Gasser, M., Fajar, N.M., Romera-Castillo, C., Pelegrí, J.L., 2014. Does a general relationship exist between fluorescent dissolved organic matter and microbial respiration? – The case of the dark equatorial. Atl. Ocean. Deep. Res. Part I Oceanogr. Res. Pap. 89, 44–55. http://dx.doi.org/10.1016/j.dsr.2014.03.007.

D'Ortenzio, F., Marullo, S., Ragni, M., D'Alcalà, M.R., Santoleri, R., 2002. Validation of empirical SeaWiFS algorithms for chlorophyll-a retrieval in the Mediterranean Sea: a case study for oligotrophic seas. Remote Sens. Environ. 82, 79–94. http://dx.doi.org/10.1016/S0034–4257(02)00026–3.

D'Sa, E.J., Steward, R.G., Vodacek, A., Blough, N.V., Phinney, D., 1999. Determining optical absorption of colored dissolved organic matter in seawater with a liquid capillary waveguide. Limnol. Oceanogr. 44, 1142–1148. http://dx.doi.org/10.4319/lo.1999.44.4.1142.

Falkowski, P.G., Raven, J.A., 1997. Aquatic Photosynthesis. Blackwell Science, Oxford, Gophen, 375 pp..

Galí, M., Simó, R., Pérez, G.L., Ruiz-González, C., Sarmento, H., Royer, S.-J., Fuentes-Lema, A., Gasol, J.M., 2013. Differential response of planktonic primary, bacterial, and dimethylsulfide production rates to static vs. dynamic light exposure in upper mixed-layer summer sea waters. Biogeosciences 10, 7983–7998. http://dx.doi.org/10.5194/bg-10–7983–2013.

Gallegos, C.L., 1994. Refining habitat requirements of submersed aquatic vegetation : role of optical models. Estuaries 17, 187–199.

Gallegos, C., 2001. Calculating optical water quality targets to restore and protect submersed aquatic vegetation: overcoming problems in partitioning the diffuse attenuation coefficient for photosynthetically active radiation. Estuaries 24, 381. http://dx.doi.org/10.2307/1353240.

Gitelson, A., Karnieli, A., Goldman, N., Yacobi, Y.Z., Mayo, M., 1996. Chlorophyll estimation in the Southeastern Mediterranean using CZCS images: adaptation

of an algorithm and its validation. J. Mar. Syst. 9, 283–290.
Gordon, H.R., Morel, A., 1983. Remote sensing of ocean color for interpretation of satellite visible imagery: a review. In: Barber, R.T., Mooers, C.N.K., Bowman, M.J. (Eds.), Zeitzschel. Lecture Notes on Coastal and Estuarine Studies.Springer-Verlag, New York, pp. 1–114.
Helms, J.R., Stubbins, A., Ritchie, J.D., Minor, E.C., Kieber, D.J., Mopper, K., 2008. Absorption spectral slopes and slope ratios as indicators of molecular weight, source, and photobleaching of chromophoric dissolved organic matter. Limnol. Oceanogr. 53, 955–969. http://dx.doi.org/10.4319/lo.2008.53.3.0955.
Hu, C., Lee, Z., Muller-Karger, F.E., Carder, K.L., Walsh, J.J., 2006. Ocean color reveals phase shift between marine plants and yellow substance. IEEE Geosci. Remote Sens. Lett. 3, 262–266. http://dx.doi.org/10.1109/LGRS.2005.862527.
IOCCG, 2000. Remote sensing of ocean color in coastal and other optically-complex waters. In: Sathyendranath, S. (Ed.), Report of the International Ocean Color Coordinating Group No. 3. IOCCG, Dartmouth, Canada, p. 145.
Kirk, J.T.O., 1981. Monte Carlo study of the nature of the underwater light field in, and the relationships between optical properties of, turbid yellow waters. Aust. J. Mar. Freshw. Res. 32, 517–532.
Kirk, J.T.O., 1984. Dependence of relationship between inherent and apparent optical properties of water on solar altitude. Limnol. Oceanogr. 29, 350–356. http://dx.doi.org/10.4319/lo.1984.29.2.0350.
Kirk, J.T.O., 1991. Volume scattering function, average cosines, and the underwater light field. Limnol. Oceanogr. 36, 455–467. http://dx.doi.org/10.4319/lo.1991.36.3.0455.
Kirk, J.T.O., 2011. Light and Photosynthesis in Aquatic Eco-Systems. Cambridge University Press, Cambridge, p. 649.
Kishino, M., Takahashi, N., Okami, N., Ichimura, S., 1985. Estimation of the spectral absorption coefficients of phytoplankton in the sea. Bull. Mar. Sci. 37, 634–642.
Kitidis, V., Uher, G., Mantoura, R.F.C., Spyres, G., 2006. Photochemical production of ammonium in the oligotrophic Cyprus Gyre (Eastern Mediterranean). Biogeosciences 3, 439–449.
Laurion, I., Ventura, M., Catalan, J., Psenner, R., Sommaruga, R., 2000. Attenuation of ultraviolet radiation in mountain lakes: factors controlling the among- and within-lake variability. Limnol. Oceanogr. 45, 1274–1288. http://dx.doi.org/10.4319/lo.2000.45.6.1274.
Lee, Z.P., Carder, K.L., Marra, J., Steward, R.G., Perry, M.J., 1996. Estimating primary production at depth from remote sensing. Appl. Opt. 35, 463–474. http://dx.doi.org/10.1364/AO.35.000463.
Lee, Z.P., Darecki, M., Carder, K.L., Davis, C.O., Stramski, D., Rhea, W.J., 2005. Diffuse attenuation coefficient of downwelling irradiance : an evaluation of remote sensing methods. J. Geophys. Res. 110, 1–9.
Lefèvre, N., Taylor, A.H., Gilbert, F.J., Geider, R.J., 2003. Modeling carbon to nitrogen and carbon to chlorophyll a ratios in the ocean at low latitudes: evaluation of the role of physiological plasticity. Limnol. Oceanogr. 48, 1796–1807.
Lewis, M., Carr, M.E., Feldman, G.C., Esaias, W., McClain, C., 1990. Influence of penetrating solar radiation on the heat budget of the equatorial Pacific Ocean. Nature 347, 543–545.
Loisel, H., Morel, A., 1998. Light scattering and chlorophyll concentration in case 1 waters : a reexamination. Limnol. Oceanogr. 43, 847–858.
Loisel, H., Vantrepotte, V., Norkvist, K., Mériaux, X., Kheireddine, M., Ras, J., Pujo-Pay, M., Combet, Y., Leblanc, K., Dall'Olmo, G., Mauriac, R., Dessailly, D., Moutin, T., 2011. Characterization of the bio-optical anomaly and diurnal variability of particulate matter, as seen from scattering and backscattering coefficients, in ultra-oligotrophic eddies of the Mediterranean Sea. Biogeosciences 8, 3295–3317. http://dx.doi.org/10.5194/bg-8-3295–2011.
Loiselle, S.A., Bracchini, L., Dattilo, A.M., Ricci, M., Tognazzi, A., Cézar, A., Rossi, C., 2009. The optical characterization of chromophoric dissolved organic matter using wavelength distribution of absorption spectral slopes. Limnol. Oceanogr. 54, 590–597. http://dx.doi.org/10.4319/lo.2009.54.2.0590.
MacIntyre, H.L., Lomas, M.W., Cornwell, J., Suggett, D.J., Gobler, C.J., Koch, E.W., Kana, T.M., 2004. Mediation of benthic–pelagic coupling by microphytobenthos: an energy- and material-based model for initiation of blooms of Aureococcus anophagefferens. Harmful Algae 3, 403–437. http://dx.doi.org/10.1016/j.hal.2004.05.005.
Miles, C.J., Bell, T.G., Lenton, T.M., 2009. Testing the relationship between the solar radiation dose and surface DMS concentrations using in situ data. Biogeosciences 6, 1927–1934. http://dx.doi.org/10.5194/bg-6-1927–2009.
Miller, R.L., Belz, M., Del Castillo, C., Trzaska, R., 2002. Determining CDOM absorption spectra in diverse coastal environments using a multiple pathlength, liquid core waveguide system. Cont. Shelf Res. 22, 1301–1310. http://dx.doi.org/10.1016/S0278–4343(02)00009–2.
Mitchell, B.G., Kiefer, D.A., 1984. Determination of absorption and fluorescence excitation spectra for phytoplankton. In: Holm-Hansen, O. (Ed.), Marine Phytoplankton and Productivity. Springer, Berlin, pp. 157–169.
Mitchell, B., Holm-Hansen, O., 1991. Bio-optical properties of Antarctic Peninsula waters: differentiation from temperate ocean models. Deep Sea Res. Part A. Oceanogr. Res. Pap. 38, 1009–1028. http://dx.doi.org/10.1016/0198–0149(91)90094-V.
Mitchell, B.G., et al., 2000. Determination of spectral absorption coefficients of particles, dissolved material and phytoplankton for discrete water samples. In: Fargion, G., Mueller, J., (Eds.), Ocean Optics Protocols (NASA/TM) Greenbelt, Maryland, pp. 125–153.
Mopper, K., Xianliang, Z., Kieber, R., et al., 1991. Photochemical degradation of dissolved organic carbon and its impact on the oceanic carbon cycle. Nature, 353.
Moran, M.A., Zepp, R.G., 1997. Review Role of photoreactions in the formation of biologically compounds from dissolved organic matter. Limnol. Oceanogr. 42, 1307–1316. http://dx.doi.org/10.4319/lo.1997.42.6.1307.
Morán, X.A.G., Estrada, M., 2005. Winter pelagic photosynthesis in the NW Mediterranean. Deep Sea Res. Part I Oceanogr. Res. Pap. 52, 1806–1822. http://dx.doi.org/10.1016/j.dsr.2005.05.009.
Morel, A., Prieur, L., 1977. Analysis of variations in ocean color. Limnol. Oceanogr. 22, 709–722. http://dx.doi.org/10.4319/lo.1977.22.4.0709.
Morel, A., 1988. Optical modeling of the upper ocean in relation to its biogenous matter content (case I waters). J. Geophys. Res. 93, 10749. http://dx.doi.org/10.1029/JC093iC09p10749.
Morel, A., Antoine, D., 1994. Heating rate within the upper ocean in relation to its bio–optical state. J. Phys. Oceanogr. 24, 1552–1665, doi:10.1175/1520–0485(1994)024 < 1652:HRWTUO > 2.0.CO;2.
Morel, A., Maritorena, S., 2001. Bio-optical properties of oceanic waters : a reappraisal. J. Geiphysical Res. 106, 7163–7180.
Morel, A., Gentili, B., 2004. Radiation transport within oceanic (case 1) water. J. Geophys. Res. 109, C06008. http://dx.doi.org/10.1029/2003JC002259.
Morel, A., Claustre, H., Antoine, D., Gentili, B., 2007a. Natural variability of bio-optical properties in Case 1 waters: attenuation and reflectance within the visible and near-UV spectral domains, as observed in South Pacific and Mediterranean waters. Biogeosciences 4, 913–925. http://dx.doi.org/10.5194/bg-4-913–2007.
Morel, A., Gentili, B., Claustre, H., Babin, M., Bricaud, A., Ras, J., Tièche, F., 2007a. Optical properties of the "clearest" natural waters. Limnol. Oceanogr. 52, 217–229, doi:0.4319/lo.2007.52.1.0217.
Morel, A., Huot, Y., Gentili, B., Werdell, P.J., Hooker, S.B., Franz, B. a, 2007b. Examining the consistency of products derived from various ocean color sensors in open ocean (Case 1) waters in the perspective of a multi-sensor approach. Remote Sens. Environ. 111, 69–88. http://dx.doi.org/10.1016/j.rse.2007.03.012.
Morel, A., 2009. Are the empirical relationships describing the bio-optical properties of case 1 waters consistent and internally compatible? J. Geophys. Res. 114, C01016. http://dx.doi.org/10.1029/2008JC004803.
Morel, A., Gentili, B., 2009a. A simple band ratio technique to quantify the colored dissolved and detrital organic material from ocean color remotely sensed data. Remote Sens. Environ. 113, 998–1011. http://dx.doi.org/10.1016/j.rse.2009.01.008.
Morel, A., Gentili, B., 2009b. The dissolved yellow substance and the shades of blue in the Mediterranean Sea. Biogeosciences 6, 2625–2636. http://dx.doi.org/10.5194/bg-6-2625–2009.
Mueller, J.L., Austin, R.W., 1995. Ocean optics protocols for SeaWIFS validation, Review 1. NASA Technical Memo. 104566, 67 pp.
Mueller, J.L., Morel, A., Frouin, R., Davis, C.O., Arnone, R.A., Carder, K.L., Lee, Z., Steward, R.G., Hooker, S.B., Mobley, C.D., McLean, S., Holben, B.N., Miller, M., Pietras, C., Knobelspiesse, K.D., Fargion, G.S., Porter, J., Voss, J.L., 2003. Ocean optics protocols for satellite ocean color sensor validation, revision 4, volume III: radiometric measurements and data analysis protocols. Ocean Opt. Protoc. Satell. Ocean Color Sens. Valid. Revis. 4 (III), 78.
Nayar, S., Chou, L.M., 2003. Relative efficiencies of different filters in retaining phytoplankton for pigment and productivity studies. Estuar. Coast. Shelf Sci. 58, 241–248. http://dx.doi.org/10.1016/S0272–7714(03)00075–1.
Nelson, N.B., Siegel, D.A., Michaels, A.F., 1998. Seasonal dynamics of colored dissolved material in the Sargasso Sea. Deep Sea Res. Part I: Oceanogr. Res. Pap. 45, 931–957.
Nelson, N.B., Siegel, D.A., Carlson, C. a, Swan, C.M., 2010. Tracing global biogeochemical cycles and meridional overturning circulation using chromophoric dissolved organic matter. Geophys. Res. Lett. 37. http://dx.doi.org/10.1029/2009GL042325, n/a–n/a.
Nelson, N.B., Siegel, D.A., 2013. The global distribution and dynamics of chromophoric dissolved organic matter. Ann. Rev. Mar. Sci. 5, 447–476. http://dx.doi.org/10.1146/annurev-marine-120710-100751.
Organelli, E., Bricaud, A., Antoine, D., Matsuoka, A., 2014. Seasonal dynamics of light absorption by chromophoric dissolved organic matter (CDOM) in the NW Mediterranean Sea (BOUSSOLE site). Deep Sea Res. Part I Oceanogr. Res. Pap. 91, 72–85. http://dx.doi.org/10.1016/j.dsr.2014.05.003.
Oubelkheir, K., Claustre, H., Sciandra, A., Babin, M., 2005. Bio-optical and biogeochemical properties of different trophic regimes in oceanic waters. Limnol. Oceanogr. 50, 1795–1809. http://dx.doi.org/10.4319/lo.2005.50.6.1795.
O'Reilly, J.E., Maritorena, S., Mitchell, B.G., Siegel, D.A., Carder, K.L., Garver, S.A., Kahru, M., McClain, C.R., 1998. Ocean color chlorophyll algorithms for SeaWiFS. J. Geophys. Res. 103, 24937–24953. http://dx.doi.org/10.1029/98JC02160.
Para, J., Coble, P.G., Charrière, B., Tedetti, M., Fontana, C., Sempéré, R., 2010. Fluorescence and absorption properties of chromophoric dissolved organic matter (CDOM) in coastal surface waters of the northwestern Mediterranean Sea, influence of the Rhône River. Biogeosciences, 7, pp. 4083–4103, ⟨http://dx.doi.org/10.5194/bg-7-4083-2010⟩.
Pierson, D.C., Kratzer, S., Strömbeck, N., Håkansson, B., 2008. Relationship between the attenuation of downwelling irradiance at 490 nm with the attenuation of PAR (400 nm–700 nm) in the Baltic Sea. Remote Sens. Environ. 112, 668–680. http://dx.doi.org/10.1016/j.rse.2007.06.009.
Platt, T., Sathyendranath, S., Caverhill, C.M., Lewis, M.R., 1988. Ocean primary production and available light: further algorithms for remote sensing. Deep Sea Res. Part A Oceanogr. Res. Pap. 35, 855–879. http://dx.doi.org/10.1016/0198–0149(88)90064–7.
Pope, R.M., Fry, E.S., 1997. Pure water. II. Integrating cavity measurements. Appl. Opt. 36, 8710–8723.
Prieur, L., Sathyendranath, S., 1981. An optical classification of coastal and oceanic waters based on the specific spectral absorption curves of phytoplankton

pigments, dissolved organic matter, and other particulate materials. Limnol. Oceanogr. 26, 671–689.
Quillon, S., Petrenko, A., 2005. Above-water measurements of reflectance and chlorophyll-a algorithms in the Gulf of Lions. Opt. Express 13, 2531–2548.
Roesler, C.S., Boss, E., 2003. Spectral beam attenuation coefficient retrieved from ocean color inversion. Geophys. Res. Lett. 30, 1–4. http://dx.doi.org/10.1029/2002GL016185.
Romera-Castillo, C., Sarmento, H., Alvarez-Salgado, X. a, Gasol, J.M., Marrase, C., 2010. Production of chromophoric dissolved organic matter by marine phytoplankton. Limnol. Oceanogr. 55, 446–454. http://dx.doi.org/10.4319/lo.2010.55.1.0446.
Romera-Castillo, C., Nieto-Cid, M., Castro, C.G., Marrasé, C., Largier, J., Barton, E.D., Álvarez-Salgado, X.A., 2011. Fluorescence: absorption coefficient ratio – tracing photochemical and microbial degradation processes affecting coloured dissolved organic matter in a coastal system. Mar. Chem. 125, 26–38. http://dx.doi.org/10.1016/j.marchem.2011.02.001.
Romera-Castillo, C., Álvarez-Salgado, X.A., Galí, M., Gasol, J.M., Marrasé, C., 2013. Combined effect of light exposure and microbial activity on distinct dissolved organic matter pools. A seasonal field study in an oligotrophic coastal system (Blanes Bay, NW Mediterranean). Mar. Chem. 148, 44–51. http://dx.doi.org/10.1016/j.marchem.2012.10.004.
Röttgers, R., Doerffer, R., 2007. Measurements of optical absorption by chromophoric dissolved organic matter using a point-source integrating-cavity absorption meter. Limnol. Oceanogr. Methods 5, 126–135. http://dx.doi.org/10.4319/lom.2007.5.126.
Siegel, D.A., Mitchaels, A.F., 1996. Quantification of non-alagal light attenuation in the Sargasso Sea. Deep Sea Res. Part II Top. Stud. Oceano. 43, 321–345.
Siegel, D.A., Maritorena, S., Hansell, D.A., Lorenzi-Kayser, M., 2002. Global distribution and dynamics of colored dissolved and detrital organic materials. J. Geophys. Res. 107, 1–14. http://dx.doi.org/10.1029/2001JC000965.
Siegel, D.A., Maritorena, S., Nelson, N.B., Behrenfeld, M.J., McClain, C.R., 2005. Colored dissolved organic matter and its influence on the satellite-based characterization of the ocean biosphere. Geophys. Res. Lett. 32, L20605. http://dx.doi.org/10.1029/2005GL024310.
Simon, A., Shanmugam, P., 2013. A new model for the vertical spectral diffuse attenuation coefficient of downwelling irradiance in turbid coastal waters: validation with in situ measurements. Opt. Express 21, 543–545. http://dx.doi.org/10.1364/OE.21.030082.
Six, C., Finkel, Z.V., Irwin, A.J., Campbell, D. a, 2007. Light variability illuminates niche-partitioning among marine Picocyanobacteria. PLoS One 2, e1341. http://dx.doi.org/10.1371/journal.pone.0001341.
Smith, A.R.C., Marra, J., Perry, M.J., Baker, K.S., Swift, E., Buskey, E., Jolla, L., 1989. Estimation of a Photon Budget for the Upper Ocean in the Sargasso Sea Estimation of a photon budget for the upper ocean in the Sargasso Sea. Limnol. Oceanogr. 34, 1673–1693.
Stæhr, P.A., Markager, S., 2004. Parameterization of the chlorophyll a -specific in vivo light absorption coefficient covering estuarine, coastal and oceanic waters. Int. J. Remote Sens. 25, 5117–5130. http://dx.doi.org/10.1080/01431160410001716932.
Suresh, T., Talaulikar, M., Desa, E., Mascarenhas, A., 2012. Comparison of measured and satellite derived spectral diffuse attenuation coefficients for the Arabian Sea. Int. J. Environ. Remote Sens 33, 570–585. http://dx.doi.org/10.1080/01431161.2010.543435.
Smyth, T.J., Tilstone, G.H., Groom, S.B., 2005. Integration of radiative transfer into satellite models of ocean primary production. J. Geophys. Res. C Ocean 110, 1–11. http://dx.doi.org/10.1029/2004JC002784.
Tilstone, G.H., Smyth, T.J., Gowen, R.J., Martinez-Vicente, V., Groom, S.B., 2005. Inherent optical properties of the Irish Sea and their effect on satellite primary production algorithms. J. Plankton Res. 27, 1127–1148. http://dx.doi.org/10.1093/plankt/fbi075.
Tilstone, G.H., Taylor, B.H., Blondeau-Patissier, D., Powell, T., Groom, S.B., Rees, A.P., Lucas, M.I., 2015. Comparison of new and primary production models using SeaWiFS data in contrasting hydrographic zones of the northern North Atlantic. Remote Sens. Environ. 156, 473–489. http://dx.doi.org/10.1016/j.rse.2014.10.013.
Twardowski, M.S., Boss, E., Sullivan, J.M., Donaghay, P.L., 2004. Modeling the spectral shape of absorption by chromophoric dissolved organic matter. Mar. Chem. 89, 69–88. http://dx.doi.org/10.1016/j.marchem.2004.02.008.
Tyler, J.E., 1975. The in situ quantum efficiency of natural phytoplankton populations. Limnol. Oceanogr. 20, 976–980. http://dx.doi.org/10.4319/lo.1975.20.6.0976.
Uitz, J., Claustre, H., Morel, A., Hooker, S.B., 2006. Vertical distribution of phytoplankton communities in open ocean: An assessment based on surface chlorophyll. J. Geophys. Res. 111, 1–23. http://dx.doi.org/10.1029/2005JC003207.
Vallina, S.M., Simó, R., 2007. Strong relationship between DMS and the solar radiation dose over the global surface ocean. Science 315, 506–508. http://dx.doi.org/10.1126/science.1133680.
Vähätalo, A.V., Zepp, R.G., 2005. Photochemical mineralization of dissolved organic nitrogen to ammonium in the Baltic Sea. Environ. Sci. Technol. 39, 6985–6992. http://dx.doi.org/10.1021/es050142z.
Vignudelli, S., Santinelli, C., Murru, E., Nannicini, L., Seritti, a, 2004. Distributions of dissolved organic carbon (DOC) and chromophoric dissolved organic matter (CDOM) in coastal waters of the northern Tyrrhenian Sea (Italy). Estuar. Coast. Shelf Sci. 60, 133–149. http://dx.doi.org/10.1016/j.ecss.2003.11.023.
Volpe, G., Santoleri, R., Vellucci, V., Ribera d'Alcalà, M., Marullo, S., D'Ortenzio, F., 2007. The colour of the Mediterranean Sea: global versus regional bio-optical algorithms evaluation and implication for satellite chlorophyll estimates. Remote Sens. Environ. 107, 625–638. http://dx.doi.org/10.1016/j.rse.2006.10.017.
Voss, K.J., 1992. A spectral model of the beam attenuation coefficient in the ocean and coastal areas. Limnol. Oceanogr. 37, 501–509.
Wang, G., CAO, W., Yang, D., Xu, D., 2008. Variation in downwelling diffuse attenuation coefficient in the northern South China Sea. Chinese J. Oceanol. Limnol. 26, 323–333.
Xing, X., Morel, A., Claustre, H., D'Ortenzio, F., Poteau, A., 2012. Combined processing and mutual interpretation of radiometry and fluorometry from autonomous profiling Bio-Argo floats: 2. Colored dissolved organic matter absorption retrieval. J. Geophys. Res. Ocean 117, 1–16. http://dx.doi.org/10.1029/2011JC007632.
Xing, X., Claustre, H., Wang, H., Poteau, A., D'Ortenzio, F., 2014. Seasonal dynamics in colored dissolved organic matter in the Mediterranean Sea: Patterns and drivers. Deep Sea Res. Part I Oceanogr. Res. Pap. 83, 93–101. http://dx.doi.org/10.1016/j.dsr.2013.09.008.
Yuan, X., Zhou, W., Huang, H., Yuan, T., et al., 2016. Bacterial influence on chromophoric dissolved organic matter in coastal waters of the northern South China Sea. Aquat. Micro. Ecol. 76, 207–217. http://dx.doi.org/10.3354/ame01778.
Zapata, M., Rodriguezl, F., Garrido, J.L., 2000. Separation of chlorophylls and carotenoids from marine phytoplankton : a new HPLC method using a reversed phase C8 column and pyridine- containing mobile phases. Mar. Ecol. Prog. Ser. 195, 29–45.
Zhang, Y.L., Liu, M.L., Wang, X., Zhu, G.W., Chen, W.M., 2009. Bio-optical properties and estimation of the optically active substances in Lake Tianmuhu in summer. Int. J. Remote Sens. 30, 2837–2857. http://dx.doi.org/10.1080/01431160802558592.